A trade-off between stress resistance and tolerance underlies the adaptive response to hydrogen peroxide

Basile Jacquel[1*], Bor Kavčič[2,3], Audrey Matifas[4], Thomas Julou[2,3], Gilles Charvin[1*]

Affiliations:

1) *GMGM UMR 7156, Université de Strasbourg, CNRS, Strasbourg, France*
2) *Biozentrum, University of Basel, Basel, Switzerland*
3) *Swiss Institute of Bioinformatics, Basel, Switzerland*

4) *IGBMC UMR7104, Université de Strasbourg, CNRS, INSERM, Illkirch, France*

*: Corresponding authors: charvin@igbmc.fr, jacquelb@igbmc.fr

Abstract

Cells employ two different defense strategies against environmental stress: resistance, aimed at preserving cell proliferation by degrading the stressor, and tolerance, focused on ensuring cell survival, even at the expense of proliferation. These strategies are complementary, yet whether they are coordinated to ensure an optimal physiological stress response remains unknown. Here, we used microfluidics and live cell imaging to explore the genetic basis of the interplay between resistance and tolerance during the response to hydrogen peroxide (H_2O_2) in budding yeast. Our analysis unraveled that, among antioxidants, some were clearly associated with resistance while others contribute to tolerance. Furthermore, we found that the *zwf1*Δ mutant, responsible for NADPH synthesis via the PPP pathway, exhibited a decrease in resistance that was counterbalanced by an unexpected exacerbation of tolerance to H_2O_2, thus revealing a trade-off that we further observed in *E. coli*. Our results support a model in which redox signaling triggers the switch to a nutrients-dependent non-proliferative tolerant state via inhibition of protein kinase A when the H_2O_2 homeostatic response is overwhelmed. Our framework could help develop synergistic therapies that target both resistance and tolerance mechanisms to prevent drug-escape mechanisms and disease relapse.

Introduction

Cell responses to stress are complex and involve a variety of mechanisms that promote physiological adaptation in changing environments. A broad class of defense mechanisms against both environmental and endogenous insults uses sense-and-respond regulatory systems based on the homeostatic framework. Many such mechanisms have been described with exquisite molecular detail, like as the oxidative stress response [1–3] and the response to hyperosmolarity [4]. In this framework, cells attempt to restore a preexisting

optimal cellular state by removing the cause of internal stress. The role of the homeostatic system is thus to ensure the maintenance of proliferation despite the presence of external disturbances, i.e., to reach a state of "stress resistance"[5,6]. Whereas such regulatory mechanisms may drive excellent adaptive properties at steady-state [7–9], they often suffer from a number of limitations, including a limited homeostatic range and a slow response time. For example, slow transcriptional activation[7,10] can restrict the cell's ability to deal with abrupt unpredictable environmental changes.

An alternative defense scheme called "stress tolerance" [5], has been described whereby a population of cells can survive a transient physiological threat without necessarily fighting the intrinsic cause of internal stress. In this framework, cell survival is usually associated with arrested proliferation and reduced metabolism, as commonly observed in the context of cellular dormancy [11], or in specific cases of heterogeneous cellular behavior such as bacterial persistence [12,13] or bet-hedging [14,15]. Stress response strategies can thus be split into those that seek to maintain cell proliferation under stress (resistance) versus those that ensure cell survival (tolerance). The former may *a priori* maximize cellular fitness; however, their intrinsic limitations expose the cells to damage and death. In the latter, cell survival usually comes at the cost of reduced cellular proliferation and offers only temporary protection against stress exposure.

Even though these two strategies might thus complement each other to provide a more versatile stress response, they are usually investigated in separate biological frameworks: studies focusing on homeostatic regulatory mechanisms generally overlook the existence of stress tolerance (which stands beyond the homeostatic framework by definition). Conversely, stress tolerance has been primarily studied in response to xenobiotic stressors against which cells cannot elicit any specific stress response [5,16]. Thus, whether mechanisms that mediate resistance and tolerance do coexist and how they are coordinated to optimize cell fitness in response to an environmental stressor is largely unknown.

Redox homeostasis is an essential feature for cells to function properly when facing redox perturbations of external and internal origin [1,2]. In yeast, the Yap1 regulon controls hydrogen peroxide (H_2O_2) levels through a canonical sense-and-respond system [17–19]: upon H_2O_2 exposure, the Yap1 transcription factor drives the expression of about one hundred genes [17,20,21], including antioxidant enzymes with somewhat overlapping H_2O_2 scavenging functions [22–26]. Additional regulations contribute to the restoration of internal H_2O_2 balance: first, glycolysis rerouting to the pentose phosphate pathway (PPP) leads to increased production of NADPH [27,28], which is the ultimate electron donor involved in H_2O_2 buffering in the peroxidatic cycle [29]; additionally, the inhibition of the protein kinase A (PKA) pathway, which is a major hub for cell proliferation control [30,31] and the general stress response [21,32], contributes to the adaptation to oxidative stress[33] and is connected to the H_2O_2 signaling response through various putative mechanisms [34–37]. Therefore, the response to H_2O_2 in yeast provides an ideal context for studying how resistance and tolerance mechanisms are shaping an integrative stress response.

To address this question, we used live-cell imaging and microfluidics approaches to develop combined proliferation and survival assays that can distinguish between H_2O_2-resistant and tolerant cellular behaviors. Using a candidate-gene screen, we classified the main players involved in H_2O_2 stress response into functional categories that highlight their respective

roles in adaptation to this stressor. Specifically, our study revealed the existence of a strong antagonism between resistance and tolerance, which was exacerbated by mutations that affect NADPH fueling in the peroxidatic cycle in budding yeast (e.g., *zwf1*Δ and *trr1*Δ mutants), a phenomenon that appeared to be conserved in *E. coli* when mutating the zwf gene. Further analyses unraveled the role of PKA regulation and the availability of nutrients in orchestrating the interplay between resistance and tolerance upon exposure to H_2O_2. This model system paves the way for developing anti-proliferative strategies in which both resistance and tolerance mechanisms could be independently targeted to improve therapeutic efficiency.

Results

Resistance and tolerance are distinct physiological properties of the hydrogen peroxide stress response

Classical stress response assays often fail to distinguish the cell's ability to maintain proliferation (i.e., resistance) and its capacity to survive to a given stress exposure (i.e., tolerance). To make this distinction, we developed two independent microfluidics-based single-cell time-lapse assays: in the first experiment, we monitored the proliferation of individual cells and their progeny in the presence of a constant concentration of H_2O_2 (i.e. resistance assay, see Fig. 1a). We measured the fraction of resistant cells in response to increased concentrations of H_2O_2 (Fig. 1b). This assay revealed a sharp decline in cell proliferation above a ~0.7mM concentration (referred to as the minimum inhibitory concentration, or MIC, see Fig. 1b)). In the second experiment, we measured cell survival (i.e., tolerance assay, see Fig. 1c) by quantifying the fraction of cells already present at the onset of stress exposure that were able to recover proliferation following a stress exposure of a given duration. Plotting the fraction of tolerant cells versus the duration of stress (Fig. 1d) revealed a sharp decay in survival with increasing durations, the rate of which was [H_2O_2]-dependent and could be quantified by calculating the MDK99 (or Minimal Duration to Kill 99% of the population, Extended Data Fig. 1a). Notably, despite a noticeable death rate on a short timescale, the survival of cells exposed to a H_2O_2 concentration below the MIC (i.e., 0.5mM) plateaued after 2 hours of exposure, likely due to the maintained proliferation of a fraction of resistant cells in the population. Therefore, under these conditions, cells display different phenotypes (i.e. resistant, tolerant or dead), suggesting that both tolerance and resistance mechanisms co-exist within the population.

Yet, strikingly, above the MIC, cells could survive a stress exposure even though they were unable to resist at that concentration. For instance, ~10% of the population survived following a 1h exposure at 1mM (see Fig. 1d), even though much less than 1% of the cells could grow at this concentration (Fig. 1b). Therefore, resistance and tolerance appear as related yet distinct cellular properties of the response to hydrogen peroxide.

The Yap1-mediated transcriptional stress response is required for H_2O_2 resistance but not for H_2O_2 tolerance

According to the homeostatic framework, the adaptation of the cells to hydrogen peroxide is in part mediated by the activation of the transcriptional activation of the Yap1 regulon. To check whether this mechanism was responsible for resistance, tolerance, or both, we

assayed and quantified the mean cellular expression of the Yap1-dependent transcriptional reporter Srx1pr-GFP-degron (*SRX1* encodes a sulfiredoxin and is tightly regulated by Yap1, Extended Data Fig. 1b-d) over time in response to exposure to increasing doses of H_2O_2 (Fig. 1e). We found that the mean peak expression (measured at 1 hour) increased with [H_2O_2] for small doses (<0.2mM, see Fig. 1f, black curve) but then decreased to zero for concentrations higher than 0.3mM. This suggests that the cells could no longer activate the main transcriptional program at those intermediate H_2O_2 concentrations. To further quantify this observation, we computed the stress response capacity, that we defined as the normalized difference between the observed peak response and the expected response after extrapolating the Srx1pr-GFP data observed at low doses (<0.2mM), see inset and blue curve in Fig. 1f. Strikingly, this analysis revealed that the decline in stress response capacity with increasing [H_2O_2] coincided with that of resistance, but not of tolerance (Figure 1g).

To further investigate the link between resistance, tolerance, and the Yap1-mediated transcriptional activation, we took advantage of the cell-to-cell heterogeneity in antioxidant response and cell fate within the population. To do this, we defined a threshold of Srx1pr-GFP fluorescence to identify cells that were able to induce an antioxidant response (referred to as “responders” in the following, see Extended Data Fig. 1e,f and Methods). As expected, the fraction of responders declined with [H_2O_2] above 0.3mM (Extended Data Fig. 1f), consistently with the observed decay in stress response capacity at the population level. Based on this analysis, we found that all the resistant cells were responders (Fig. 1h, and Extended Data Fig. 1g,h), indicating that the transcriptional response of the Yap1 regulon is necessary for resistance. Also, resistant cells had a significantly larger antioxidant expression than the non-resistant cells (Figure 1h, S1g and S1h), but no such correlation existed for tolerance upon a 1mM H_2O_2 exposure (Fig. 1i, Extended Data Fig.1 i,j). Altogether, these experiments suggest that stress resistance, but not tolerance, is mediated by the Yap1-mediated transcriptional response triggered by stress exposure.

Investigating the genetic determinism of resistance and tolerance unravels a trade-off between stress resistance and stress tolerance

We then sought to investigate the genetic determinism of resistance and tolerance. Based on the above results, we were particularly interested in testing which among the genes controlled by Yap1 were driving these two aspects of H_2O_2 defense. We also included mutants that were extensively described as stress sensitive in the literature (see Extended Data Fig. 2a for the list of mutants). We systematically measured the proliferation (i.e., by quantifying the total biomass production during a 4-hour interval, see Material and Methods) and survival of mutants in response to a 0.5mM H_2O_2 exposure (Fig. 2a, top panel and Extended Data Fig. 2b). In addition to the step stress patterns, we used ramping stress of similar magnitude, since it significantly reduces the observed drop in cell proliferation upon stress exposure and greatly enhances cell survival in the WT (see Fig. 2a and Extended Data Fig 2c). This effect is most likely due to the fact that ramps eliminate the deleterious effects of an acute stress exposure by providing more time to the homeostatic to kick in [7]. Hence, by eliminating the short-term cell death upon stress exposure, ramps may allow for more relevant comparative measurements (i.e., mutants vs WT) of resistance at steady-state during stress exposure.

To validate this methodology, first, we checked that *yap1*Δ and the *gsh1*Δ mutants (*GSH1* encodes an enzyme involved in the biosynthesis of glutathione) displayed no proliferation and tolerance in both stepping and ramping stress, in agreement with their constitutive role for general redox homeostasis and other canonical cellular functions [18], see Fig. 2b and Extended Data Fig. 2c. Then, our analysis unraveled a group of mutants with a strong resistance defect compared to the WT (R1 rectangle on Fig. 2b). This group included the genes that ensure a functional peroxidatic cycle (referred as the Prx/Trx pathway, see schematic in Fig. 2c), which is orchestrated by enzymes called 2-cys peroxiredoxins (i.e. Tsa1, Tsa2, and Ahp1; the triple mutant is referred to as *3Prx*Δ on Fig. 2b). Peroxireodxins drive the reduction of H_2O_2 and are recycled by thioredoxins (Trx1,2), which are themselves reduced by the NADPH-dependent Thioredoxin reductase (Trr1) [38]. NADPH is mostly synthesized in the Pentose Phosphate Pathway, the first step of which is ensured by the glucose-6-phosphate dehydrogenase (or G6PDH, which is encoded by the *ZWF1* gene) [39]. Importantly, all these mutants (and the combination thereof) displayed a consistent decrease in resistance, suggesting that, as expected, any impairment in this pathway is detrimental to restore an internal H_2O_2 balance.

In contrast, neither the deletion of the cytoplasmic catalase (Ctt1) nor the Cytochrome C peroxidase (Ccp1) nor the sulfiredoxin Srx1 (which reduces the hyperoxidated form of peroxiredoxins) did significantly affect cell resistance (Fig. 2b). Similarly, inhibiting the general stress response by deleting *MSN2/4* transcription factors, or the yeast kinase *YAK1* (that mediates in part the PKA-dependent activation of Msn2 [40]), or hyper-activating the Protein Kinase A (PKA) pathway by deleting *PDE2* - both interventions have been shown to make cells sensitive to H_2O_2 [33,41]- did not yield a strong reduction in resistance. Instead, all these genes displayed a more significant decrease in cell tolerance compared to the WT upon stepping stress (see T1 and T2 groups on Fig. 2b). In short, this analysis thus demonstrates that among the genes involved in the response to oxidative stress, some are crucial to restoring or maintaining proliferation, while others rather contribute to cell survival.

To refine this distinction between pro-resistance and pro-tolerance genes, we hypothesized that the ability of the cells to restore a physiological internal H_2O_2 balance upon stress exposure would be impaired in mutants with a decreased resistance. To check this, we used the Srx1pr-GFP-deg reporter as a proxy for H_2O_2 balance, assuming that the decline in fluorescence following the peak expression faithfully reveals the deactivation of the Yap1 transcription due to a drop in internal H_2O_2 concentration, as previously described [7]. We integrated this reporter in all the mutants reported above and, for each strain, we quantified the ability of the cells to restore the H_2O_2 balance by computing the "H_2O_2 restoration index" (or HRI, see Methods for details) in response to a 0.1mM H_2O_2 step stress (Extended Data Fig. 2d,e). The HRI was defined as the ratio between the mean cytoplasmic fluorescence at t=1 hour (i.e. corresponding to the peak Srx1pr-GFP-degron level in the WT under these conditions) and that at t=5 hours. Thus, higher HRIs indicate a better ability to restore the internal H_2O_2 balance. By normalizing the HRI of each mutant to that of the WT, we observed that poorly resistant mutants (R1 group) were all impaired in their ability to scavenge H_2O_2 (Fig. 2d). Instead, tolerance mutants in the T1 and T2 groups seemed less affected (Fig. 2d). Overall, we found a correlation coefficient of 0.88 between HRI and resistance (Fig. 2d), thus confirming the link between the ability to degrade H_2O_2 and to maintain cell proliferation under stress. In contrast, we found no positive correlation between HRI and tolerance (correlation coefficient = -0.55, Fig. 2e).

Apart to the previously mentioned gene clusters, our focus was drawn to two mutants *zwf1Δ* and *trr1Δ.* These mutants exhibited diminished resistance and a low HRI, aligning with the other factors regulating the peroxidatic cycle (depicted as R1 genes on Fig. 2b,d). However, we measured a remarkable 3- and 5-fold increase in tolerance compared to the WT, respectively (Fig. 2b). This was quite unexpected since these mutants were previously described as sensitive to H_2O_2 in various model organisms [28,42–46]. Further stress response assays revealed that the MIC of the *zwf1*Δ mutant was indeed significantly lower than that of the WT (0.3mM and 0.7mM, respectively, Fig. 2f,1b). Additionally, this mutant exhibited an increased survival fraction at all tested concentrations (ranging from 1 to 64mM) for durations equal to half the WT's MDK_{99} (Fig. 2g, left panel), with a mean fold survival of 4.62 +/- 2.09 compared to the WT strain (Fig. 2g, right panel). Therefore, our analysis of candidate genes unraveled two mutants, *zwf1*Δ and *trr1*Δ, in which a pronounced H_2O_2 resistance defect, together with a loss of H_2O_2 homeostasis, was associated with an unexpected hyper-tolerant phenotype over a broad range of conditions.

Proliferation and survival are antagonistic features of the oxidative stress response

We then sought to characterize further how the mutation of the *ZWF1* gene induces both a decline in proliferation under H_2O_2 stress and an increase in tolerance, and whether this effect depends on the internal H_2O_2 balance.

We first asked whether the transcriptional response of the Yap1 regulon was impaired in the mutant. To do this, we quantified the expression of the Srx1pr-GFP-deg reporter, in response to mild concentrations of H_2O_2 ranging from 0.05mM to 0.2mM (i.e. below the MIC of the *zwf1Δ* mutant). Our results indicated that the mutant displays a mean peak expression level similar to that of the WT (Fig. 3a and Extended Data Fig. 3a), suggesting that the mutant's resistance defect is not due to a lack of activation of the regulon. Instead, unlike the WT, these experiments confirmed that the mutant fails to restore the H_2O_2 balance, as evidenced by the persistent activation of the Srx1pr reporter (Fig. 3a) and nuclear localization of the Yap1-sfGFP fusion (Extended Data Fig. 4b,c). Notably, increasing H_2O_2 concentrations lead to a larger activation of the Yap1 regulon that correlates negatively with growth rate at steady state (i.e., at t=5 hours after the onset of stress exposure, Fig. 3b and Extended Data Fig. 3d,e). This negative correlation was also present for single cells at steady state within a population exposed to a 0.1mM H_2O_2 stress (Fig. 3c): under these conditions, there was a large cell-cell heterogeneity that clearly indicated that the slowly dividing cells had a high Srx1pr-GFP expression (r(*zwf1*Δ) = -0.70, see Fig. 3b). In addition, even in the absence of stress, *zwf1*Δ cells underwent sporadic reversible activations of the Yap1 regulon that coincided with a transient arrest of cell division (Extended Data Fig. 3f). Altogether, these results suggest that the *zwf1*Δ mutation leads to a large yet heterogeneous and fluctuating H_2O_2 imbalance that in turn induces a reduction in cell proliferation.

To investigate further the impact of H_2O_2 imbalance on cellular function, we investigated the level of proteome oxidation in the *zwf1*Δ mutant. To do this, first, we monitored the formation of fluorescence foci of Tsa1-GFP fusion in cells exposed to a 0.5mM H_2O_2 over 8 hours. Indeed, Tsa1 has been shown to undergo supramolecular assemblies when super-oxidized in response to severe H_2O_2 levels[47,48]. In the WT, we observed and quantified the progressive appearance of Tsa1-GFP foci in response to stress in the population of cells, followed by a decrease that was likely due to the adaptation to stress. Instead, in the *zwf1*Δ mutant, the

onset of aggregation was much faster and irreversible over a continuous 8-hour stress exposure (see Extended Data Fig. 3g and Methods). We obtained similar results with the Hsp104-GFP fusion (Extended Data Fig. 3h), which was used as a generic marker of protein aggregation (Hsp104 is a disaggregase that binds misfolded aggregated proteins, and is known to form localized foci in response to H_2O_2[49]. These experiments provided evidence that the H_2O_2 imbalance in the *zwf1*Δ mutant drives the stable appearance of hallmarks of proteome oxidation.

Next, to determine how protein oxidation is linked to cell proliferation, we released cells exposed to 0.5mM H_2O_2 over 16 hours into a medium without stress and we scored the dynamics of protein aggregation using an Hsp104-GFP reporter (Fig. 3d and 3e). Strikingly, we observed a progressive disaggregation of Hsp104-GFP that temporally coincided with cell cycle re-entry in the cells that survived the stress (Figure 3d and 3e and Extended Data Fig. 3i). This suggested that the recovery of cell proliferation requires the reduction of the proteome. In further support of this, adding 5mM DTT (a protein reducing compound) to the medium upon H_2O_2 stress release significantly accelerated both the disappearance of aggregates and cell cycle re-entry. Altogether, these experiments demonstrated that protein oxidation observed upon stress exposure in the *zwf1*Δ mutant is tightly associated with proliferation arrest, yet it is reversible and does not impair the ability of the cells to recover growth upon stress removal. Hence, this suggests that, like the internal H_2O_2 imbalance, proteome oxidation is not necessarily detrimental to cell survival in the *zwf1*Δ background.

To further investigate this hypothesis, we used the large intrinsic cell-to-cell variability in H_2O_2 balance in the *zwf1Δ* mutant to ask how the initial H_2O_2 balance affects cell survival after a severe stress pulse. To do this, we submitted the cells to a 7.5min-long 64mM H_2O_2 exposure and we scored the fraction of surviving cells as a function of the initial Srx1-GFP expression level (see left panel on Fig. 3f). We discovered that the initial imbalance in internal H_2O_2 is a very good predictor of survival to a future acute H_2O_2 stress exposure ($r = 0.96$ on binned data, see right panel on Fig. 3f): cells with a large initial imbalance display an improved stress tolerance. Altogether, this analysis unraveled that, in the *zwf1*Δ mutant, increasing the H_2O_2 imbalance by impairing the homeostatic function causes antagonistic effects on cellular resistance and tolerance. Hence it suggests the existence of a mechanism that signals the H_2O_2 imbalance to shut down growth control and to drive protective effects on cellular function, despite high internal oxidation levels.

Stress tolerance requires the Prx/Trx pathway to drive PKA inhibition

Genetic perturbations that maintain a high PKA activity during stress exposure have long been observed to induce a significant stress sensitivity[30]. In agreement with this, our candidate-gene approach confirmed that the general stress response and PKA inhibition were specifically required for H_2O_2 tolerance (see *pde2*Δ and *msn2/4*Δ mutants on Fig. 2b). In the following, we thus asked whether the control of PKA activation was involved in the trade-off observed between low resistance and high tolerance in the *zwf1*Δ mutant. For this, we used a *pde2*Δ mutant and we also prepared media supplemented with cAMP to exacerbate the effect of the mutation, as previously described[50].

We first quantified the nuclear shuttling of an Msn2-GFP fusion as a readout of PKA activation. We found that the transient nuclear relocation of Msn2-GFP in response to a

0.5mM H_2O_2 step was greatly decreased in the *pde2*Δ strain compared to the WT, in agreement with a robust PKA activation (see Fig 4a,b and Extended Data Fig. 4a). In contrast, in the *zwf1*Δ mutant, Msn2-GFP remained nuclear at all times during stress exposure, consistently with a strong PKA inhibition (Fig. 4a,c). Adding the *pde2*Δ mutation to the *zwf1*Δ background made Msn2-GFP fully cytoplasmic during stress exposure (Fig. 4b,c and Extended Data Fig. 4a), suggesting that PKA was indeed reactivated in that strain.

Then, to directly check whether constitutive PKA activation could rescue the impaired cell growth of the *zwf1*Δ mutant upon stress exposure, we measured the budding rate of the double mutant at steady-state along with its H_2O_2 imbalance (using an Srx1pr-GFP-deg reporter) during H_2O_2 exposure at concentrations ranging from 0 to 0.2mM. We found that deleting *PDE2* in a *zwf1*Δ context did not restore the H_2O_2 balance, as expected. Yet it significantly improved the proliferation during stress exposure compared to the *zwf1*Δ mutant (Figure 4d). This observation further demonstrates that the resistance defect in the *zwf1*Δ mutant upon H_2O_2 exposure is at least in part a regulated process, as it cannot simply be the consequence of reduced proliferation due to putative cellular damages.

Based on these observations, we hypothesized that the PKA-driven growth inhibition in the *zwf1*Δ mutant might also control H_2O_2 tolerance. Using a 0.5mM H_2O_2 step survival assay, we found that the *pde2*Δ deletion was indeed epistatic to *zwf1Δ* for survival (Fig. 4e), and this result was confirmed using higher stress concentrations (Extended Data Fig. 4b). Moreover, using a stress ramping assay amplified the genetic interactions between *pde2*Δ and *zwf1*Δ: although both *pde2*Δ and *zwf1*Δ single mutants had a high survival fraction in ramp assays, the vast majority of the *pde2*Δ *zwf1*Δ cells died, and this effect was exacerbated when cAMP was added to the medium (Fig. 4f). Altogether, these results demonstrate that the H_2O_2 hyper-tolerance observed in the *zwf1*Δ mutant requires PKA inhibition.

How is the internal H_2O_2 signal relayed to mediate PKA inhibition in response to stress? Recent studies have proposed that peroxiredoxins in their oxidized form (or, alternatively, thioredoxins) may inactivate PKA through a redox-dependent mechanism [36,37]. To further evaluate this model in the context of stress tolerance, we investigated whether the deletion of thioredoxins or peroxiredoxins would be epistatic to the *zwf1*Δ mutant in survival assays. Upon exposure to a 0.5mM H_2O_2 stress step exposure, we found that the hyper-tolerant phenotype of both the *zwf1*Δ and *trr1*Δ mutants was suppressed when combined with the *trx1/2*Δ mutations (Fig. 4g). Similarly, knocking out all three peroxiredoxins *TSA1*, *TSA2*, and *AHP1* (*3Prx*Δ) abolished the hyper-tolerant phenotype of the *zwf1Δ* mutant, but not the knockout of *TSA1* alone (Fig. 4g). In line with that, the quantification of nuclear Msn2-GFP localization confirmed that PKA was no longer inhibited in the *trx1/2Δ zwf1Δ* mutant under stress, but this inhibition persisted in the *tsa1*Δ *zwf1*Δ mutant (Extended Data Fig. 4c). Importantly, these results provide evidence that the increased tolerance observed in the *zwf1*Δ and *trr1*Δ mutants is due to the activation of redox signaling relay and is not simply the consequence of the reduced growth-rate of these mutants.

Altogether, this genetic analysis reveals that the control of PKA activation is an essential determinant of cell fate in response to H_2O_2 stress: PKA inhibition promotes cell survival, at the cost of limiting cell proliferation (i.e. resistance). Conversely, maintaining a high PKA activity enhances cell resistance to a mild stress, but is detrimental to cell survival at

intermediate or high stress levels. Importantly, upon stress exposure, our results indicate that the peroxiredoxin pathway not only promotes cell resistance by scavenging H_2O_2, but it also mediates PKA inhibition to ensure H_2O_2 tolerance via its redox signaling function. Hence, the peroxiredoxin pathway plays a central role in the decision-making process leading to antagonistic cell fates (i.e. resistance versus tolerance) depending on the magnitude of the H_2O_2 imbalance (Fig. 4h).

Stress tolerance restricts cell death in glucose-depleted cells, despite their inability to maintain H_2O_2 homeostasis

If the peroxiredoxin pathway-mediated switch controls cell fate in response to internal H_2O_2 stress, we reasoned that modulating the nutrients availability may impact the decision made by the cells between resistance and tolerance. To test this hypothesis, we took advantage of the constant medium replenishment in the microfluidic device to grow the cells in varying steady glucose concentrations ranging from 2% to 10^{-5}%, which modulated the budding rate from 0.014 to 0.004 min^{-1} , respectively, see the black curve on Fig. 5a. In these conditions, a small 0.1mM H_2O_2 stress induced a [glucose]-dependent decline in the budding rate at steady-state: although cells could perfectly adapt to this stress concentration at 2%, the growth rate was permanently reduced at lower glucose concentration compared to the no stress condition (see blue curve on Fig. 5a). Similarly, upon an intermediate 0.5mM H_2O_2 stress exposure, the reduction of glucose concentration from 2% to 10^{-5}% induced a dramatic decrease in the fraction of resistant cells (Fig. 5b).

To check whether this drop in resistance was associated with both a failure to induce the Yap1 regulon and to ensure the internal H_2O_2 balance, we quantified the response of a strain carrying an Srx1pr-GFP-deg reporter in response to a 0.1mM H_2O_2 stress in cells growing with various concentrations of glucose. We found that lower nutrients levels induced a reduction in the promoter's peak expression (Extended Data Fig. 5a), associated with a more pronounced H_2O_2 imbalance at steady state, measured as a ~2.5 fold reduction of the HRI from 2% to 10^{-5}% glucose (Extended Data Fig. 5a and 5c). Hence our results demonstrate that a loss of efficacy of the H_2O_2 homeostasis system accompanies the drop in resistance under low glucose concentrations.

Yet, the reduction in glucose concentration led to a significant increase in survival in response to a 64mM H_2O_2 stress, ranging from ~0.05 at 2% glucose to around 0.6 for glucose concentrations >10^{-3}%, see Fig. 5e. Interestingly, our analysis also revealed a sweet-spot at which cells exhibited both an increased resistance (Fig. 5b) and tolerance (Fig. 5d) to H_2O_2. This could be due to the fact that, at a 0.01% glucose concentration, cells might conserve an NADPH level high enough to scavenge H_2O_2 while benefiting from a reduced PKA signaling leading to increased tolerance. Altogether, these results indicate that glucose concentration dramatically affects the cellular strategy in response to H_2O_2.

The trade-off between H_2O_2 resistance and tolerance in G6PDH-deficient cells is conserved in the prokaryote *E. coli*

The redox homeostatic system, including both the Prx cycle and the PPP as the main source of NADPH, is highly conserved in other organisms [29,44,51]. In the prokaryote *E. coli*, rerouting of glucose into the PPP in response to H_2O_2 is a key metabolic adaptation [45]. We thus thought to explore whether the trade-off between resistance and tolerance revealed by the

*zwf1*Δ and *trr1*Δ mutants in *S. cerevisiae* between resistance and tolerance was also conserved in *E. coli*. Mutants deleted for *zwf* (G6PDH, ortholog of *ZWF1* in budding yeast) or *trxB* (thioredoxin reductase, ortholog of *TRR1* in budding yeast) gene had a lower growth rate than the WT (Extended Data Fig. 6a), in agreement with a reduced NADPH level and/or reduced H_2O_2 scavenging. We next used an improved mother machine microfluidics device (Fig. 6a top panel, also see Methods) to assess the response to H_2O_2 of these mutants (Fig. 6b and Extended Data Fig. 6b). Below the MIC (until 0.25 mM for WT and Δ*zwf* and 0.2 mM for Δ*trxB*, Extended Data Fig. 6c), we found that resistant Δ*zwf* cells but not resistant Δ*trxB* cells elicited reduced proliferation (normalized by no stress control) compared to the WT (Fig. 6c, also see Methods). Indeed, while the growth rate of WT and Δ*zwf* cells was similarly affected by the treatment at 0.05 mM (see Fig. 6d left panel, median normalized growth rate = 0,98 and 0,99 for WT and Δ*zwf* respectively, $p>0.05$), two subpopulations were observed at 0.25 mM, with a significantly higher fraction of cells exhibiting very low growth rate in the mutant (Fig 6d, right panel, median normalized growth rate = 0,71 and 0,32 for WT and Δ*zwf* respectively, $p<0.0001$). Yet, strikingly, the Δ*zwf* mutant (but not Δ*trxB*) had a greater survival fraction than the WT at higher H_2O_2 concentrations (Fig. 6e), highlighting its increased tolerance. Altogether, these results demonstrate that the trade-off between H_2O_2 resistance and tolerance is conserved in the Δ*zwf* but not in the Δ*trxB* mutant in *E. coli*.

Discussion

In this study, we sought to uncover the intricate ways in which cells orchestrate diverse defense strategies to ensure their adaptation in challenging environments. For that, we investigated the cellular response to hydrogen peroxide stress in yeast, focusing on the regulation of resistance and tolerance as two distinct, yet complementary defense strategies. We developed microfluidics-based assays to distinguish them and examined their respective genetic determinants. Our analysis revealed that the Yap1-mediated transcriptional response is essential for resistance but not tolerance (Fig. 1). Through a systematic analysis of mutants, we further showed that mutants associated with the Prx/Trx recycling pathway and NADPHsynthesis exhibited decreased resistance, underscoring the importance of redox homeostasis in promoting resistance (Fig. 2). Strikingly, we found that deleting *ZWF1* (and its ortholog zwf in E. coli) or *TRR1* genes, required for NADPH production and the NADPH-dependent reduction of thioredoxin respectively, unraveled an unexpected trade-off with reduced resistance but increased tolerance. We further showed that this trade-off is controlled by a Prx/Trx-dependent redox signaling that inhibits PKA depending on the maintenance of redox homeostasis in cells.

Based on these findings, we propose a model in which the cell's commitment to a defined H_2O_2 response strategy is based on the real-time assessment of the oxidation level of the components of the Prx/Trx pathway. Cellular resistance is an optimal choice under either low H_2O_2 levels or when H_2O_2 levels are progressively increased (i.e. ramping stress), because the H_2O_2 homeostatic system can efficiently degrade the stressor. In contrast, in response to acute H_2O_2 steps larger than 0.6mM, tolerance is the primary defense mechanism. The decision-making between these two defense strategies is the cornerstone that shapes the overall response to H_2O_2: resistance aims at maximizing cellular fitness by limiting cellular damages and therefore ensuring cell growth, while a prerequisite for tolerance is the downregulation of cell growth. Thus, this study provides a unique example of a stress response strategy based on a tradeoff between growth and survival.

Classical H_2O_2 “sensitivity” measurements with assays using solid media supplemented with hydrogen peroxide can not discriminate between resistance and tolerance because both proliferation and survival influence the overall cellular fitness and biomass production. This may explain why the hyper-tolerant phenotype of the *trr1*Δ and *zwf1*Δ mutant was not picked up in previous studies [28,42–46,52]. In contrast, longitudinal cell analyses based on live imaging, as performed in our study, or complementary approaches to score cell growth and survival separately [53], provide an adequate framework to discriminate among the different possible fates in response to stress.

By providing a quantitative assessment of the contribution of genes involved in the H_2O_2 stress response, our study underlines their non-redundancy: in contrast to the Prx/Trx pathway which drives H_2O_2 scavenging and hence are the key players ensuring cellular resistance, NADPH-independent cytochrome c peroxidase (*CCP1*) and catalase T (*CTT1*) contribute significantly to H_2O_2 tolerance, while playing a minor role in resistance. These distinct physiological functions might be explained by their biochemical properties: Prx are highly efficient enzymes under low fluxes of H_2O_2 while catalases are much more efficient under high H_2O_2 fluxes *in vitro* [38]. Similarly, *msn2/4*Δ and *pde2*Δ mutants displayed a reduced tolerance but no resistance defect, suggesting that the general stress response pathway may play a specific role in cell survival, but is not involved in the H_2O_2 homeostatic regulation as previously suggested [54]. Upon severe H_2O_2 exposures (until ~100 times the MIC), at which transcription-dependent mechanisms are abolished, it is likely that other mechanisms contribute to cellular tolerance. For instance, rapid protein complex formations such as protein aggregation [55] or phase separation [56] are central for stress survival in other contexts. In our study, the large and fully reversible formation of protein aggregates colocalizing with the chaperone protein Hsp104 is compatible with this observation (Fig. 3). Specifically, the PKA pathway regulates the formation of various protein complexes such as stress granules [57,58], that contain key regulators of growth. We therefore hypothesize that tolerance depends, at least in part, on rapid protein complex formations that might protect the growth machinery and avoid their irreversible oxidation upon severe internal [H_2O_2].

Growth arrest is largely described upon stress exposure and is controlled at multiple levels [30,59]. However, it is often unclear whether growth arrest is the fact of stress toxicity or rather a regulated cellular process and whether it participates in stress survival [59,60]. Here, the growth rate decreased proportionally to internal H_2O_2 imbalance in the *zwf1*Δ mutant and was partially rescued by deleted *PDE2*, thus arguing in favor of a regulatory process at play via the PKA growth pathway. Indeed, how PKA is regulated upon H_2O_2 exposure has been recently refined by providing genetic and biochemical evidence that its inhibition is mediated either by peroxiredoxins [36,37] or thioredoxins [61], which relay H_2O_2 signals and physically interact with PKA subunits [36,37]. In particular, the central role of Tsa1 and more generally peroxiredoxins as H_2O_2 relay signaling molecules [62] somewhat contributed to toning down its importance as an H_2O_2 scavenging enzyme. Here, our results emphasize that both functions - namely H_2O_2 scavenging and redox signaling - are equally important: the peroxidase function is essential for homeostatic system function and hence resistance, whereas Prx and Trx signaling to PKA is the key mechanism that drives tolerance. Importantly, this dual function explains how the antagonism between H_2O_2 resistance and tolerance is anchored at the molecular level; in their reduced form, the peroxidase function of Prx sustains resistance, while their oxidized form drives the shutdown of PKA to reinforce tolerance [37,62]. Thus, our work gives a perspective on how redox signaling controls cell physiology in response to

H_2O_2, orchestrating the trade-off between stress resistance and tolerance. Interestingly, coordinating stress defense strategy with H_2O_2 homeostasis (via the Prx/Trx-PKA relay) might enhance the overall cell fitness in fluctuating environments, by restricting growth shutdown to situations in which cell survival is threatened. These data are consistent with recent findings showing that Yap1 mediates a fast and direct response to H_2O_2, while Msn2/4 dictates a slower general stress response [63], presumably protecting cells from H_2O_2 toxicity through broader cellular modifications (such as growth shutdown[31]) when the antioxidant H_2O_2-scavenging is insufficient.

Resource allocation in response to stress is indeed critical for cells and affects both their fitness [64,65] and their stress response [66]. In our study, limiting glucose availability dramatically changed the defense strategy of cells, turning them to a hyper tolerant phenotype, in line with the long-standing increased stress survival in starved cells [13,67,68]. However, we found that limited glucose availability was also associated with reduced H_2O_2 scavenging. This suggests that quiescent cells may survive harsh stressors in an '*out-of-homeostasis*' state thanks to protective mechanisms limiting the toxicity of H_2O_2. In this view, tolerance appears as a last resort defense strategy, avoiding cell death when internal homeostasis is lost, and resistance precluded.

Extending our study to E. coli revealed the partial conservation of the resistance-tolerance trade-off in Δ*zwf* (ortholog of *ZWF1*) but not in Δ*trxB* (ortholog of *TRR1*). If it is unclear why the trxB mutant didn't exhibit the trade-off, we speculate that part of the *zwf* tolerance phenotype might depend on NADPH-dependent but Prx/Trx-independent processes in *E. coli*, such as the antioxidant glutathione [69] or anabolic processes [46]. Most importantly, we provide evidence that the PPP-dependent NADPH production is an evolutionary conserved determinant of H_2O_2-defense strategy in eukaryotes and prokaryotes. Exploring whether such trade-off exists in other microorganisms and in response to other stressors could unravel a universal stress defense organization.

Tolerance recently appeared as a central mechanism in antibiotic treatment failures [6,7071] and is associated with specific stress response mechanisms [67,72]. However, studies that focus on physiological homeostatic systems instead try to understand the determinants of resistance [4,73–75]. Our analysis of the H_2O_2 stress response shows that resistance and tolerance are indeed intertwined elements with overlapping molecular bases, both of which contributing to cellular fitness. Most importantly, mutations that impair resistance (e.g., *zwf1*Δ) do not necessarily affect tolerance and may even enhance it. Conversely, targeting tolerance by preventing PKA inhibition (e.g., like in the *pde2*Δ mutant) does not necessarily impair cellular resistance (pde2Δ mutant has no growth defect in H_2O_2 ramps). However, altering both resistance and tolerance leads to a strong fitness defect no matter the temporal stress profile (see Fig. 4). Many therapeutic strategies attempt to impair cellular functions by targeting cellular proliferation (i.e. resistance). Yet, powerful tolerance mechanisms can be responsible for relapses after the treatment. Targeting both defense strategies could provide an avenue to prevent treatments relapse.

Methods

Strains and plasmids

All budding yeast strains were congenic to the S288C background (Sikorski and Hieter, 1989; Huh et al., 2003) and derived from BY4741 or BY4742. The list of strains is detailed in Supplementary file 1. Simple mutant strains were all taken from the BY4742 delta collection (invitrogen). The *trx1*Δ *trx2*Δ and the *tsa1*Δ*tsa2*Δ*ahp1*Δ strains were gifts from the Toledano Lab and were also derived from S288c. The strain *msn2*Δ*msn4*Δ was a gift from *Dr.* Li Wei and was also derived from S288c*.* All strains have been genotyped by PCR. The transcriptional reporter strains carrying the *SRX1pr-sfGFP-deg* were generated by a one-step cloning-free method (Huber et al., 2014) in the corresponding mutant strain issued from the BY4742 delta collection (invitrogen). The double mutants (*X*Δ *zwf1*Δ*::natMX4*) were obtained by substituting the entire *ZWF1* gene by a natMX4 cassette in the corresponding *X*Δ*::kanMX4* strain from the BY4742 delta collection (invitrogen). The mutants *tsa1*Δ*tsa2*Δ*ahp1*Δ*zwf1*Δ*::natMX4, trx1*Δ*trx2*Δ*zwf1*Δ*::natMX4* and *trx1*Δ*trx2*Δ*trr1*Δ*::natMX4* were obtained following the same procedure, substituting the *ZWF1* or the *TRR1* gene by a natMX4 cassette in the corresponding strain. The protein fusion GFP strains were obtained from the BY4741 Invitrogen collection. The strains HSP104-GFP *zwf1*Δ*::natMX4 and* SRX1-GFP *zwf1*Δ*::natMX4* were obtained by substituting the entire *ZWF1* gene by a natMX4 cassette in the corresponding protein fusion GFP strain (from invitrogen).

For bacterial strains, the ortholog of yeast thioredoxin reductase trr1 and of zwf1 in *E. coli* are *trxB* and *zwf* respectively. The Δ*trxB* strain was obtained from the KEIO library [76,77]. The Δ*zwf* strain of the collection was incorrect, and was therefore constructed from scratch. After verification by sequencing, it was moved into BW25113 using generalized P1 transduction. Deletions of *trxB* and *zwf* were confirmed by PCR and subsequent Sanger sequencing (Microsynth) using locus-specific primers. Additionally, we transformed BW25113 with a low-copy plasmid pUA66-hi2GFP bearing synthetic-promoter-driven GFP to monitor the occurrence of lysis (detected as sudden loss of GFP content). We refer to this strain as “WT.”

Microfabrication and microfluidics setup

The microfluidic chips design for yeast cell experiments was the same as that in Goulev et al., eLife, 2017. Microfluidics chips were PDMS (Sylgard 184,10:1 mixing ratio) replicas of the master mold. The chip was covalently bonded to a 24 × 50 mm coverslip using a Plasma activator (Diener, Germany). The microfluidic chip was connected to a peristaltic pump (Ismatec, Switzerland) within one hour following the plasma activation with Teflon tubing. The rate of the pump was set between 20 and 60 μL/min. Linear ramps of medium containing H_2O_2 were done as described in Goulev et al., Methods Cell Biol 2018.

For *E. coli* experiments, we modified the design of the “mother machine” microfluidic device so as to let media flow through the growth channels while retaining cells. To do so, we added shallow structures (0.35μm) around the growth channel and connected those to another flow channel at the back, as described elsewhere [78]*.* To ensure rapid and controlled switching between conditions, we utilized the same “dial-a-wave” mixer from the DIMM device described earlier [79], although without mixing serpentine since we only used one media input

or the other; as previously, the chip is designed in order to perform experiments with 8 strains and/or pairs of media in parallel. We manufactured the devices using standard methods of soft lithography. After cutting the chip and punching inlets, the chip was bonded to a pre-cleaned glass coverslip (Schott, TD_00134) by air plasma activation (20-25 s at pressure between 15-20 Pa, power 'High' on plasma cleaner PDC-32G, Harrick Plasma) immediately before assembling the chip, followed by baking for 1-1.5 h at 80ºC. We assembled the device and primed it with deionized water on the day of the experiment.

Growth medium and H_2O_2 preparation

For yeast cultures and microfluidics experiments, cells were grown at 30°C in synthetic complete 2% dextrose supplemented with amino-acids. The H_2O_2 (Hydrogen peroxide solution 35wt. % in H_2O_2, 349887–500 ML, Sigma) solutions were prepared as described in Goulev et al., eLife 2017. For *E. coli* experiments, precultures and microfluidic experiments were done at 37ºC, using filter sterilized M9 minimal medium (Sigma Aldrich, M6030), supplemented with 0.2% w/v glucose (AppliChem, A1349) and 0.1% w/v casamino acids (Sigma Aldrich, 22090). For all experiments, we added hydrogen peroxide (SigmaAldrich, 8859) to the media just before the experiment to prevent degradation in the absence of stabilizers. We stored a stock solution of hydrogen peroxide at 4ºC in the dark after opening.

Culture conditions and Time-lapse microscopy

For yeast time-lapse imaging, cells were pre-grown overnight at 30°C. Overnight cultures were then diluted and grown for 4 to 6h to mid-log phase and were injected in the microfluidics device. Cells were left to grow at least one division in the microfluidic chip before the beginning of the experiment. Images were taken using an inverted Zeiss Axio Observer Z1 or a Zeiss Axiovert. The focus was maintained using a software custom algorithm developed on MatLab. Fluorescence images were taken using a LED light (CoolLed, LumenCor) and an EM-CCD Luca-R camera (Andor) and using either a 63x objective (with Zeiss Axio Observer Z1) or a 40x objective (Zeiss Axiovert). Multi-Position imaging was enabled by an automated stage (up to 80 positions). The temperature was set to 30°C during the whole experiment using both a custom objective heater (controlled with a 5C7-195, Oven Industries) and a holder heater (controlled using a custom Arduino module).

For *E. coli* experiments, we streaked bacterial strains on LB agar plates with antibiotics from frozen glycerol stocks and incubated the plates overnight at 37ºC before the experiment. On the day of the experiment, we inoculated liquid cultures from freshly grown colonies, and harvested bacteria at OD 0.01-0.05 for loading the microfluidic device. After starting the setup and its temperature control, we let it equilibrate several hours in advance. We used a pressure controller (OB1 mk3+, Elveflow) to control the flows in the microfluidic chip during the experiment. After mounting the chip, we ran the growth medium through for 1-3 h using our standard flow of ≈ 1.6 μL/min per individual series ($1.56 - 1.44 \times 10^5$ Pa inlet pressure, -10^4 Pa vacuum). Next, we loaded cells from the flow channel outlet by (i) increasing the flow through growth channels (media inlets at 8×10^4 Pa and overflow channel at -6×10^4 Pa) and (ii) pressurizing the loading tubing using a manifold connected to the pressure controller. Increasing the pressure on the cell outlet pushed the bacteria into the growth channels. To monitor the switching between different media, we added fluorescein (Sigma Aldrich, F6377) in media containing hydrogen peroxide at a final concentration of 10 ng/mL.

An inverted Nikon Ti2-E microscope, equipped with a motorized xy-stage and enclosed in a temperature incubator (TheCube, Life Imaging Systems), was used to perform microfluidic experiments. Images were recorded using a CFI Plan Apochromat Lambda DM 100× oil objective (NA 1.45, WD 0.13 mm) and a sCMOS camera (Photometrics Kinetix); the largest possible field of view of 208 µm×208 µm (3200 pixel×3200 pixel) was obtained by using large optical elements in the light path. The setup was controlled using µManager 2 [80] and time-lapse movies were recorded with its Multidimensional-Acquisition engine, using "blanking" settings so as to illuminate the sample only during camera exposure. At each position, we acquired every 3 min a phase-contrast image using 100 ms exposure and an image of GFP fluorescence (120 ms exposure, 50% power attenuated by OD 1 filter, Lumencor Spectra 3, Cyan LED with ex 475/35 nm; em 525/50 nm; bs 495 nm filters). We chose these acquisition settings and frequency as they minimize the phototoxicity due to exposure to the short-wavelength excitation light and yet still allow for around ten acquisitions between cell divisions. For each condition-strain combination, we were able to acquire six to seven positions (around 50-60 growth channels per position).

Image analysis for yeast experiments

For budding yeast experiments, raw images were imported and processed on MatLab using a free access custom software (phyloCell, available on GitHub, Charvin 2017). The software was used to segment and track cells over time. Segmentation and tracking were then corrected manually with the phyloCell interface when needed for single-cell analysis. Camera background was systematically subtracted for all fluorescence quantifications.

Quantification of physiological and fluorescence parameters in budding yeast

Minimal inhibitory concentration (MIC)

The minimal duration to inhibit the growth of the population was routinely assessed by the incapacity of cells to recover an exponential growth within 12 h following stress exposure. No WT cells were found to recover growth after 12 h if they hadn't started recovering before that point. In addition, due to the reduced growth rate in the *zwf1Δ* mutant, we tested in three independent replicates that assessing growth recovery for 24 h instead of 12 h did not change its MIC (data not shown).

Post-stress survival fraction

For post-stress survival quantification, only cells present at the beginning of the stress were included in the analysis. Following this procedure, the post-stress survival fraction was assessed independently of the proliferative capacity of cells under stress and therefore independently of stress resistance. The survival fraction was manually measured by determining the fraction of cells (born before stress exposure) able to form at least 2 consecutive buds following stress release. Counting two buds enabled us to exclude cells that remained arrested as G2/M during their first post-stress division due to a DNA-damage checkpoint arrest (Goulev et al., 2017).

Minimal duration to kill 99% of the population (MDK99)

The MDK99 was calculated following the procedure described in the '*Post-stress survival*' section. Each independent replicate included at least one hundred cells and typically a few hundred cells. This limits the accuracy of the measurement of the survival fraction. The MDK99 of the population was assessed based on 2 to 4 independent microfluidic experiments for each condition tested.

Fold increase in cell proliferation

In the mutant screen in Fig. 2, proliferation under stress was assessed by measuring the fold change in cell number during the finite stress period for each micro-colony present at the beginning of the stress period. Importantly, only resistant cells were included in the analysis to avoid any artefactual drop in proliferation due to non-growing tolerant or dead cells. Normalized cell proliferation was then calculated by dividing the averaged proliferation obtained in the tested condition to that of the no stress WT condition.

Bud to bud frequency (or cell budding rate)

The bud to bud frequency was calculated as the inverse of the time measured between the formation of two successive buds. This readout was used as a proxy of single-cell proliferation under stress at steady-state (in Figure 3 and 4). To avoid taking into account the acute regime following H_2O_2 exposure, we excluded the budding events occurring during the first 5 hours of stress exposure. Cells exhibiting a bud-to-bud duration >10h were arbitrarily considered as non-budding cells (frequency <0.0017 min^{-1}) and therefore as non-resistant cells.

Normalized tolerance, resistance and stress response capacities

To compare how H_2O_2 tolerance, resistance and stress response behaves as a function of H_2O_2 concentration, we defined dimensionless normalized variables for tolerance and stress response. Normalized tolerance was defined as the MDK99 at a given concentration divided by the MDK99 at 1 mM (i.e. the MDK99 right above the MIC, where tolerance starts to be defined). The normalized stress response at t=1h following stress addition was defined based on the mean Srx1pr-GFP expression (see '*Quantification of the SRX1pr-GFP-deg'* section) as follows: *Normalized stress response = 1 - ((Exp - Fit) / Fit)*, where *Exp* is the experimentally measured peak expression for each [H_2O_2] and *Fit* the extrapolation of the linear fit at small doses of H_2O_2, considering a linear dose-response peak expression. Normalized resistance and stress response were then fitted using a sigmoidal function, with a half capacity obtained at very similar H_2O_2 concentrations (0.27 and 0.28 mM respectively). Tolerance was not following an exponential decay and was thus fitted using a power law.

Cell-cycle re-entry following stress exposure

Cell cycle re-entry was quantified manually, assessing the moment at which each single-cells initiated a newly formed bud after stress release; the cumulative fraction of surviving cells re-entering the cell cycle over time was then plotted (see Fig. 3e, dash line).

Quantification of the SRX1pr-GFP-deg

The SRX1pr-GFP-deg signal was quantified as the mean pixel value within the segmented cell area. Peak fluorescence was determined in each cell as the level of fluorescence at t=1h following stress addition after subtracting the initial fluorescence value in the absence of stress.

H_2O_2 Restoration Index (HRI)

The H_2O_2 restoration index (HRI) was calculated using the SRX1pr-GFP-deg quantification in single cell as the ratio of the mean GFP value 5h after the addition of a 0.1 mM H_2O_2 stress to that measured 1h after stress addition. This score was then normalized to the WT.. A small HRI thus represents a low ability to rescue redox equilibrium. The H_2O_2 concentration was chosen to ensure that every strain included in the analysis could grow and display a transcriptional response upon stress exposure.

Yap1 and Msn2 nuclear localization

Yap1-sfGFP and Msn2-GFP nuclear localization were then quantified as described in Cai et al., Nature, 2008. Briefly, the nuclear localization score was measured by the difference between the mean intensity of the 5 brightest pixels in the segmented cell and the mean intensity of all other pixels in the same segmented cell.

Quantification of Hsp104-GFP and Tsa1-GFP aggregates

The relative aggregation scores of fusion protein were quantified using the same methodology as for Yap1 and Msn2 nuclear localization scores, based on the mean intensity of the 5 brightest pixels in the segmented cells as previously described in S. Saad et al., Nat Cell Biol, 2017. We checked that the results were independent of the number of pixels used to assess the specific signal of the GFP foci. To assess the Hsp104-GFP aggregation score following stress release in the *zwf1Δ* mutant (Fig. 3d,e), we excluded dead cells based on their mean fluorescence signal to only account for the Hsp104 deaggregation of viable cells. Due to the very high GFP levels in viable cells, we excluded cells with a mean fluorescence level <1000 a.u. at the moment of stress release. The fluorescence level in viable cells was far above this threshold under H_2O_2 (see Extended Data Fig. 3h).

Prediction of H_2O_2 stress survival from pre-stress fluorescence

To evaluate how redox imbalance affects future stress exposure survival, we measured the level of the Srx1-GFP fusion proteins at the onset of a burst of 7.5 or 15 min of 64 mM H_2O_2 exposure. The mean normalized fluorescence level was used as a proxy of the redox status of cells before stress. To avoid that experiment-to-experiment variability in the fluorescence level introduced a bias in the prediction, we normalized the fluorescence by the median fluorescence signal for each experiment independently, before pooling cells from all experiments together. Cells were then sorted into 6 groups based on their normalized fluorescent value. The viable/death status of each single cell was then determined as described in the '*Post-stress survival fraction*' section and the average fraction of surviving cells in each group was plotted as a function of the normalized Srx1-GFP fluorescence level prior stress exposure.

Image analysis for *E. coli* experiments

We analyzed the micrographs time-lapses in two stages. First, in the preprocessing step, we isolated individual growth channels, and corrected for small drift experienced during the acquisition. This step created videos of individual channels as well as longitudinal kymographs of growth channels. We used the latter for manually determining the regrowth, and the former for automated image analysis. We segmented and tracked the lineage of bacterial cells until the end of the hydrogen peroxide treatment using DeepMoMA. This software builds on the foundation of the original Mother-Machine analyzer (MoMA) and will be described elsewhere. DeepMoMA utilizes convolutional neural networks for generating cell-outline hypotheses and treats cell segmentation and tracking of the cells as a joint problem. Upon solving the tracking-segmentation problem, cell statistics were exported directly (e.g., cell length, lineage, etc.) without manual curation. The software is available at https://github.com/nimwegenLab/moma/releases/tag/v0.9.6 and we used segmentation model "model_20230509_8616f16b.zip" available at https://github.com/nimwegenLab/moma-model. We estimated the growth rate before the treatment for cells observed during their whole cell cycle. We fitted a linear model to the log-transformed length time-trace vs time. We did not observe any systematic effects in unperturbed growth rate between the different locations in the microfluidic device. Day-to-day variability did not exceed the variability we observed within a single experiment, except in the case of Δ*trxB* where we observed a detectable shift in mean growth rate between replicates. To obtain the fraction of resistant cells, we identified cells that were present at the start of the oxidative stress. A cell was considered non-growing if its cumulative length did not increase by more than 1.8-fold during the treatment. In order to successfully detect the growth status for as many cells as possible, we summed the length of its two daughters if a cell divided during the treatment, and cell traces were considered until the elongation threshold was exceeded, or one of the two daughters was lost (because it left the channel). In order to quantify the reduction of growth rate during oxidative stress, we considered all cells which were observed during at least 4 consecutive time points. In order to focus only on resistant cells, we kept only cells which were labeled as resistant based on the criteria described above. We fitted a linear model to the log-transformed length time-trace vs time to estimate the growth rate, and normalized it to the mean growth rate observed before treatment for the same strain. Exposure to high levels of oxidative stress incurred cell death and lysis. While the cell debris made segmentation of cell outlines difficult, we could estimate the fraction of post-stress regrowth and thus tolerance from kymographs of the growth channels generated during preprocessing. Aided by custom Python scripts, we manually annotated the kymographs for regrowth during and after treatment.

Acknowledgments

We thank Michel Toledano for fruitful discussions, Sophie Quintin, Sandrine Morlot and Théo Aspert for careful reading of the manuscript. We thank Denis Fumagalli for media and plate preparations. BJ thanks Erwan Grandgirard and Didier Hentsch for their support with microscopy. KB acknowledges tremendous support from M. Mell with the use of deepMoMA and thanks Maria-Elisenda Alaball Pujol for help with microfluidics. KB and TJ are grateful to Erik van Nimwegen and members of his research group for generous support and

discussions, which rendered this work possible. Computations carried out by KB and TJ were partially performed at sciCORE (http://scicore.unibas.ch/) scientific computing core facility at University of Basel. This work was supported by the Fondation pour la Recherche Médicale (FRM, B.J, and G.C.), the Agence Nationale pour la Recherche (G.C.), the grant ANR-10-LABX-0030-INRT, a French State fund managed by the Agence Nationale de la Recherche under the frame program Investissements d'Avenir ANR-10-IDEX-0002-02. KB gratefully acknowledges support by a postdoctoral fellowship of the “Peter und Traudl Engelhorn Stiftung.” TJ acknowledges funding from the Swiss National Science Foundation (SNSF project 310030_197836). BJ gratefully acknowledges funding from an MDPhD student fellowship from Edilb. This project has benefited from establishing collaboration at KITP workshop “Quantitative biology of non-growing microbes” supported by NSF Grant No. PHY-1748958 and the Gordon and Betty Moore Foundation Grant No. 2919.02.

References

1. Veal, E. A., Day, A. M. & Morgan, B. A. Hydrogen peroxide sensing and signaling. *Mol. Cell* **26**, 1–14 (2007).
2. Toledano, M. B., Delaunay, A., Monceau, L. & Tacnet, F. Microbial H2O2 sensors as archetypical redox signaling modules. *Trends Biochem. Sci.* **29**, 351–357 (2004).
3. Toledano, M. B., Planson, A.-G. & Delaunay-Moisan, A. Reining in H(2)O(2) for safe signaling. *Cell* **140**, 454–456 (2010).
4. Hohmann, S. Osmotic stress signaling and osmoadaptation in yeasts. *Microbiol. Mol. Biol. Rev.* **66**, 300–372 (2002).
5. Brauner, A., Fridman, O., Gefen, O. & Balaban, N. Q. Distinguishing between resistance, tolerance and persistence to antibiotic treatment. *Nat. Rev. Microbiol.* **14**, 320–330 (2016).
6. Balaban, N. Q. *et al.* Definitions and guidelines for research on antibiotic persistence. *Nat. Rev. Microbiol.* **17**, 441–448 (2019).
7. Goulev, Y. *et al.* Nonlinear feedback drives homeostatic plasticity in H2O2 stress response. *Elife* **6**, (2017).
8. Muzzey, D., Gómez-Uribe, C. A., Mettetal, J. T. & van Oudenaarden, A. A systems-level analysis of perfect adaptation in yeast osmoregulation. *Cell* **138**, 160–171 (2009).
9. Milias-Argeitis, A. *et al.* In silico feedback for in vivo regulation of a gene expression

circuit. *Nat. Biotechnol.* **29**, 1114–1116 (2011).

10. Young, J. W., Locke, J. C. W. & Elowitz, M. B. Rate of environmental change determines stress response specificity. *Proc. Natl. Acad. Sci. U. S. A.* **110**, 4140–4145 (2013).
11. Gray, J. V. *et al.* 'Sleeping Beauty': Quiescence in Saccharomyces cerevisiae. *Microbiol. Mol. Biol. Rev.* **68**, 187–206 (2004).
12. Bigger, J. TREATMENT OF STAPHYLOCOCCAL INFECTIONS WITH PENICILLIN BY INTERMITTENT STERILISATION. *Lancet* **244**, 497–500 (1944).
13. Balaban, N. Q., Merrin, J., Chait, R., Kowalik, L. & Leibler, S. Bacterial persistence as a phenotypic switch. *Science* **305**, 1622–1625 (2004).
14. Slatkin, M. Hedging one's evolutionary bets. *Nature* **250**, 704–705 (1974).
15. Levy, S. F., Ziv, N. & Siegal, M. L. Bet Hedging in Yeast by Heterogeneous, Age-Correlated Expression of a Stress Protectant. *PLoS Biol.* **10**, e1001325 (2012).
16. Brewer, G. Persistence is key. *Nat. Rev. Cancer* **22**, 605 (2022).
17. Lee, J. *et al.* Yap1 and Skn7 control two specialized oxidative stress response regulons in yeast. *J. Biol. Chem.* **274**, 16040–16046 (1999).
18. Delaunay, A., Isnard, A. D. & Toledano, M. B. H2O2 sensing through oxidation of the Yap1 transcription factor. *Sci. STKE* **19**, 5157 (2000).
19. Kuge, S. & Jones, N. YAP1 dependent activation of TRX2 is essential for the response of Saccharomyces cerevisiae to oxidative stress by hydroperoxides. *EMBO J.* **13**, 655–664 (1994).
20. Godon, C. *et al.* The H2O2 stimulon in Saccharomyces cerevisiae. *J. Biol. Chem.* **273**, 22480–22489 (1998).
21. Gasch, A. P. *et al.* Genomic expression programs in the response of yeast cells to environmental changes. *Sci. STKE* **11**, 4241 (2000).
22. Jiang, H. & English, A. M. Phenotypic analysis of the ccp1Δ and ccp1Δ-ccp1W191F mutant strains of Saccharomyces cerevisiae indicates that cytochrome c peroxidase functions in oxidative-stress signaling. *J. Inorg. Biochem.* **100**, 1996–2008 (2006).
23. Chae, H. Z., Chung, S. J. & Rhee, S. G. Thioredoxin-dependent peroxide reductase

from yeast. *J. Biol. Chem.* **269**, 27670–27678 (1994).

24. Pedrajas, J. R., Miranda-Vizuete, A., Javanmardy, N., Gustafsson, J. A. & Spyrou, G. Mitochondria of Saccharomyces cerevisiae contain one-conserved cysteine type peroxiredoxin with thioredoxin peroxidase activity. *J. Biol. Chem.* **275**, 16296–16301 (2000).
25. Wong, C.-M., Zhou, Y., Ng, R. W. M., Kung Hf, H.-F. & Jin, D.-Y. Cooperation of yeast peroxiredoxins Tsa1p and Tsa2p in the cellular defense against oxidative and nitrosative stress. *J. Biol. Chem.* **277**, 5385–5394 (2002).
26. Iraqui, I. *et al.* Peroxiredoxin Tsa1 is the key peroxidase suppressing genome instability and protecting against cell death in Saccharomyces cerevisiae. *PLoS Genet.* **5**, e1000524 (2009).
27. Ralser, M. *et al.* Dynamic rerouting of the carbohydrate flux is key to counteracting oxidative stress. *J. Biol.* **6**, 10 (2007).
28. Kuehne, A. *et al.* Acute Activation of Oxidative Pentose Phosphate Pathway as First-Line Response to Oxidative Stress in Human Skin Cells. *Mol. Cell* **59**, 359–371 (2015).
29. Hall, A., Karplus, P. A. & Poole, L. B. Typical 2-Cys peroxiredoxins--structures, mechanisms and functions. *FEBS J.* **276**, 2469–2477 (2009).
30. Broach, J. R. Nutritional control of growth and development in yeast. *Genetics* **192**, 73–105 (2012).
31. Smith, A., Ward, M. P. & Garrett, S. Yeast PKA represses Msn2p/Msn4p-dependent gene expression to regulate growth, stress response and glycogen accumulation. *EMBO J.* **17**, 3556–3564 (1998).
32. Martínez-Pastor, M. T. *et al.* The Saccharomyces cerevisiae zinc finger proteins Msn2p and Msn4p are required for transcriptional induction through the stress response element (STRE). *EMBO J.* **15**, 2227–2235 (1996).
33. Hasan, R. *et al.* The control of the yeast H2O2 response by the Msn2/4 transcription factors. *Mol. Microbiol.* **45**, 233–241 (2002).

34. Boisnard, S. *et al.* H2O2 activates the nuclear localization of Msn2 and Maf1 through thioredoxins in Saccharomyces cerevisiae. *Eukaryot. Cell* **8**, 1429–1438 (2009).
35. Molin, M. *et al.* Life span extension and H(2)O(2) resistance elicited by caloric restriction require the peroxiredoxin Tsa1 in Saccharomyces cerevisiae. *Mol. Cell* **43**, 823–833 (2011).
36. Bodvard, K. *et al.* Light-sensing via hydrogen peroxide and a peroxiredoxin. *Nat. Commun.* **8**, 14791 (2017).
37. Roger, F. *et al.* Peroxiredoxin promotes longevity and H2O2-resistance in yeast through redox-modulation of protein kinase A. *Elife* **9**, (2020).
38. Fourquet, S., Huang, M.-E., D'Autreaux, B. & Toledano, M. B. The dual functions of thiol-based peroxidases in H2O2 scavenging and signaling. *Antioxid. Redox Signal.* **10**, 1565–1576 (2008).
39. Minard, K. I., Jennings, G. T., Loftus, T. M., Xuan, D. & McAlister-Henn, L. Sources of NADPH and expression of mammalian NADP+-specific isocitrate dehydrogenases in Saccharomyces cerevisiae. *J. Biol. Chem.* **273**, 31486–31493 (1998).
40. Lee, P., Cho, B.-R., Joo, H.-S. & Hahn, J.-S. Yeast Yak1 kinase, a bridge between PKA and stress-responsive transcription factors, Hsf1 and Msn2/Msn4. *Mol. Microbiol.* **70**, 882–895 (2008).
41. Berry, D. B. & Gasch, A. P. Stress-activated genomic expression changes serve a preparative role for impending stress in yeast. *Mol. Biol. Cell* **19**, 4580–4587 (2008).
42. Pandolfi, P. P. *et al.* Targeted disruption of the housekeeping gene encoding glucose 6-phosphate dehydrogenase (G6PD): G6PD is dispensable for pentose synthesis but essential for defense against oxidative stress. *EMBO J.* **14**, 5209–5215 (1995).
43. Izawa, S. *et al.* Importance of glucose-6-phosphate dehydrogenase in the adaptive response to hydrogen peroxide in Saccharomyces cerevisiae. *Biochem. J* **330 (Pt 2)**, 811–817 (1998).
44. Ralser, M. *et al.* Dynamic rerouting of the carbohydrate flux is key to counteracting oxidative stress. *J. Biol.* **6**, 10 (2007).

45. Christodoulou, D. *et al.* Reserve Flux Capacity in the Pentose Phosphate Pathway Enables Escherichia coli's Rapid Response to Oxidative Stress. *Cell Syst* **6**, 569–578.e7 (2018).
46. Chen, L. *et al.* NADPH production by the oxidative pentose-phosphate pathway supports folate metabolism. *Nature Metabolism* **1**, 404–415 (2019).
47. Jang, H. H. *et al.* Two enzymes in one; two yeast peroxiredoxins display oxidative stress-dependent switching from a peroxidase to a molecular chaperone function. *Cell* **117**, 625–635 (2004).
48. Hanzén, S. *et al.* Lifespan Control by Redox-Dependent Recruitment of Chaperones to Misfolded Proteins. *Cell* **166**, 140–151 (2016).
49. Erjavec, N., Larsson, L., Grantham, J. & Nyström, T. Accelerated aging and failure to segregate damaged proteins in Sir2 mutants can be suppressed by overproducing the protein aggregation-remodeling factor Hsp104p. *Genes Dev.* **21**, 2410–2421 (2007).
50. Görner, W. *et al.* Nuclear localization of the C2H2 zinc finger protein Msn2p is regulated by stress and protein kinase A activity. *Genes Dev.* **12**, 586–597 (1998).
51. Chae, H. Z. *et al.* Cloning and sequencing of thiol-specific antioxidant from mammalian brain: alkyl hydroperoxide reductase and thiol-specific antioxidant define a large family of antioxidant enzymes. *Proc. Natl. Acad. Sci. U. S. A.* **91**, 7017–7021 (1994).
52. Talwar, D. *et al.* The GAPDH redox switch safeguards reductive capacity and enables survival of stressed tumour cells. *Nat Metab* **5**, 660–676 (2023).
53. Fomenko, D. E. *et al.* Thiol peroxidases mediate specific genome-wide regulation of gene expression in response to hydrogen peroxide. *Proc. Natl. Acad. Sci. U. S. A.* **108**, 2729–2734 (2011).
54. Berry, D. B. *et al.* Multiple means to the same end: the genetic basis of acquired stress resistance in yeast. *PLoS Genet.* **7**, e1002353 (2011).
55. Saad, S. *et al.* Reversible protein aggregation is a protective mechanism to ensure cell cycle restart after stress. *Nat. Cell Biol.* **19**, 1202–1213 (2017).
56. Franzmann, T. M. *et al.* Phase separation of a yeast prion protein promotes cellular

fitness. *Science* **359**, (2018).

57. Shah, K. H., Zhang, B., Ramachandran, V. & Herman, P. K. Processing body and stress granule assembly occur by independent and differentially regulated pathways in Saccharomyces cerevisiae. *Genetics* **193**, 109–123 (2013).
58. Ramachandran, V., Shah, K. H. & Herman, P. K. The cAMP-dependent protein kinase signaling pathway is a key regulator of P body foci formation. *Mol. Cell* **43**, 973–981 (2011).
59. Zhang, H., Zhao, Y. & Zhu, J.-K. Thriving under Stress: How Plants Balance Growth and the Stress Response. *Dev. Cell* **55**, 529–543 (2020).
60. Geng, Y. *et al.* A spatio-temporal understanding of growth regulation during the salt stress response in Arabidopsis. *Plant Cell* **25**, 2132–2154 (2013).
61. Boisnard, S. *et al.* H2O2 activates the nuclear localization of Msn2 and Maf1 through thioredoxins in Saccharomyces cerevisiae. *Eukaryot. Cell* **8**, 1429–1438 (2009).
62. Stöcker, S., Maurer, M., Ruppert, T. & Dick, T. P. A role for 2-Cys peroxiredoxins in facilitating cytosolic protein thiol oxidation. *Nat. Chem. Biol.* **14**, 148–155 (2018).
63. Granados, A. A. *et al.* Distributed and dynamic intracellular organization of extracellular information. *Proc. Natl. Acad. Sci. U. S. A.* **115**, 6088–6093 (2018).
64. Mitchell, A. & Pilpel, Y. A mathematical model for adaptive prediction of environmental changes by microorganisms. *Proc. Natl. Acad. Sci. U. S. A.* **108**, 7271–7276 (2011).
65. Weiße, A. Y., Oyarzún, D. A., Danos, V. & Swain, P. S. Mechanistic links between cellular trade-offs, gene expression, and growth. *Proc. Natl. Acad. Sci. U. S. A.* **112**, E1038–47 (2015).
66. Balakrishnan, R., de Silva, R. T., Hwa, T. & Cremer, J. Suboptimal resource allocation in changing environments constrains response and growth in bacteria. *Mol. Syst. Biol.* **17**, e10597 (2021).
67. Radzikowski, J. L. *et al.* Bacterial persistence is an active σ S stress response to metabolic flux limitation. *Molecular Systems Biology* vol. 12 882 Preprint at https://doi.org/10.15252/msb.20166998 (2016).

68. Wood, T. K., Knabel, S. J. & Kwan, B. W. Bacterial persister cell formation and dormancy. *Appl. Environ. Microbiol.* **79**, 7116–7121 (2013).

69. Fahey, R. C., Brown, W. C., Adams, W. B. & Worsham, M. B. Occurrence of glutathione in bacteria. *J. Bacteriol.* **133**, 1126–1129 (1978).

70. Boeck, L. Antibiotic tolerance: targeting bacterial survival. *Curr. Opin. Microbiol.* **74**, 102328 (2023).

71. Levin-Reisman, I. *et al.* Antibiotic tolerance facilitates the evolution of resistance. *Science* **355**, 826–830 (2017).

72. Harms, A., Maisonneuve, E. & Gerdes, K. Mechanisms of bacterial persistence during stress and antibiotic exposure. *Science* **354**, (2016).

73. Mettetal, J. T., Muzzey, D., Gomez-Uribe, C. & van Oudenaarden, A. The Frequency Dependence of Osmo-Adaptation in Saccharomyces cerevisiae. *Science* vol. 319 482–484 Preprint at https://doi.org/10.1126/science.1151582 (2008).

74. Muzzey, D., Gómez-Uribe, C. A., Mettetal, J. T. & van Oudenaarden, A. A Systems-Level Analysis of Perfect Adaptation in Yeast Osmoregulation. *Cell* vol. 138 160–171 Preprint at https://doi.org/10.1016/j.cell.2009.04.047 (2009).

75. Mitchell, A., Wei, P. & Lim, W. A. Oscillatory stress stimulation uncovers an Achilles' heel of the yeast MAPK signaling network. *Science* **350**, 1379–1383 (2015).

76. Baba, T. *et al.* Construction of Escherichia coli K-12 in-frame, single-gene knockout mutants: the Keio collection. *Mol. Syst. Biol.* **2**, 2006.0008 (2006).

77. Datsenko, K. A. & Wanner, B. L. One-step inactivation of chromosomal genes in *Escherichia coli* K-12 using PCR products. *Proc. Natl. Acad. Sci. U. S. A.* **97**, 6640–6645 (2000).

78. Julou, T., Gervais, T. & van Nimwegen, E. Growth rate controls the sensitivity of gene regulatory circuits. *bioRxiv* 2022.04.03.486858 (2022) doi:10.1101/2022.04.03.486858.

79. Kaiser, M. *et al.* Monitoring single-cell gene regulation under dynamically controllable conditions with integrated microfluidics and software. *Nat. Commun.* **9**, 212 (2018).

80. Edelstein, A., Amodaj, N., Hoover, K., Vale, R. & Stuurman, N. Computer control of

microscopes using μManager. *Curr. Protoc. Mol. Biol.* **Chapter 14**, Unit14.20 (2010).

Fig. 1: Resistance and tolerance are distinct physiological properties of the hydrogen peroxide stress response

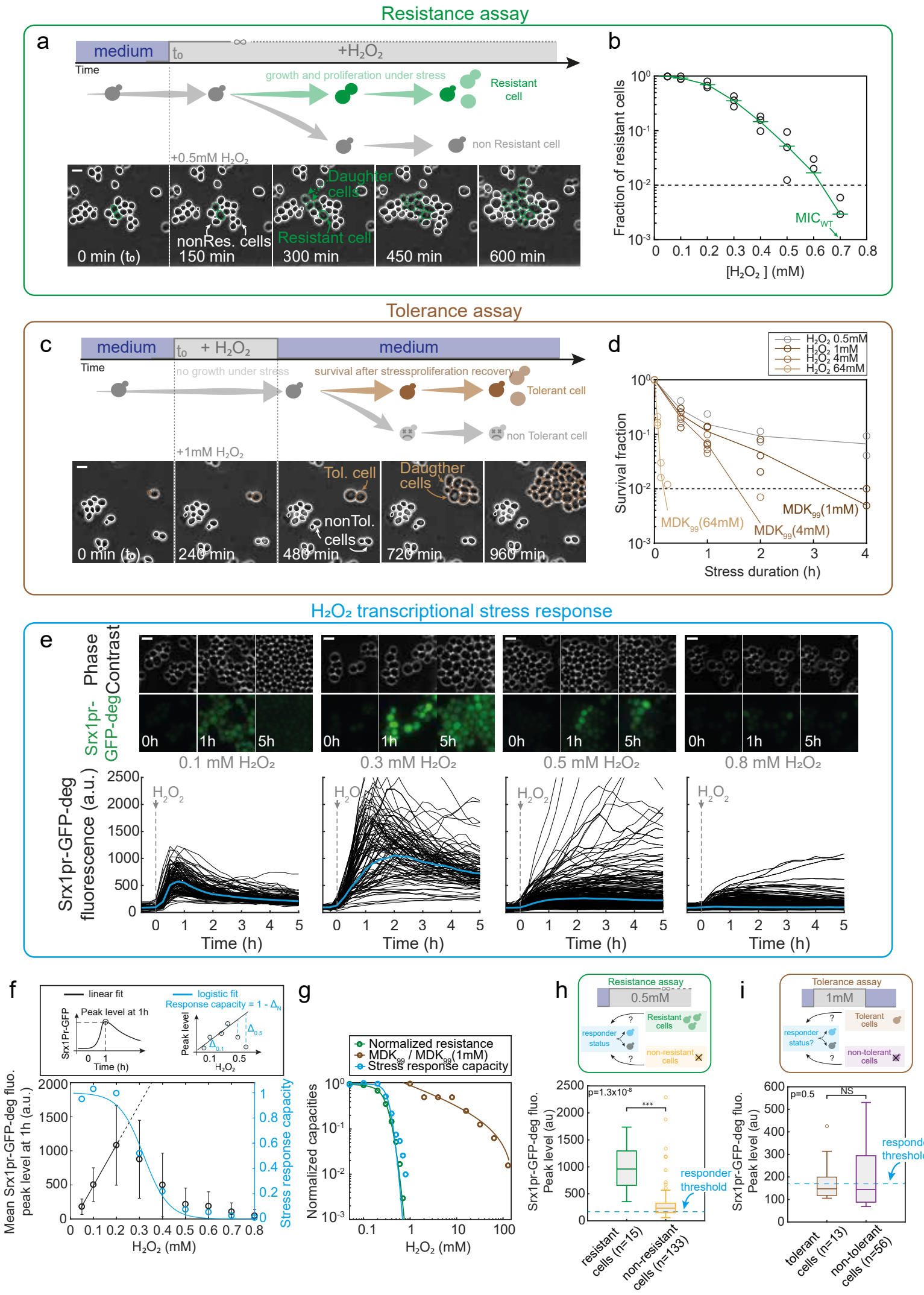

Figure 1: Resistance and tolerance are distinct properties of the response to hydrogen peroxide

a. Diagram of the resistance assay in the microfluidic device with a time series of a representative cropped field of view. Cells were exposed to 0.5 mM for an 'infinite' period of time. Green (resp. white) contours indicate resistant (resp. non resistant) cells. **b.** Fraction of resistant cells at different H_2O_2 concentration. The green arrow indicates the Minimal Inhibitory Concentration (MIC_{WT}), which is the H_2O_2 concentration where less than 1% of cells are resistant. Error bars represent the s.e.m. of N=3 technical replicates per condition (n>100 cells for each replicate). **c.** Diagram of the tolerance assay in the microfluidic device with a time series of a representative cropped field of view. Cells were exposed to a 1 mM H_2O_2 stress during 2h. Brown (resp. white) contours indicate tolerant (resp. non tolerant) cells. **d.** Survival fraction of WT cells for different stress duration and at different concentrations. Each line represents the mean survival fraction based on technical replicates (represented as circles, N = 2 or 3 per condition, n>100 for each replicate). **e.** Top: Sequence of phase contrast and fluorescence images of a SRX1pr-GFP-deg reporter strain exposed to various constant H_2O_2 concentrations. Stress addition occurs at t=0h. Bottom: representative mean single-cell GFP signals (black lines) and population median response (blue line) (n>100 cells for each condition). **f.** Top: sketch explaining how the stress response capacity is calculated; Bottom: Mean SRX1pr-GFP-deg fluorescence (+/- one standard deviation) obtained at t=1h hour following stress addition (n>500 single-cells pooled from N>2 technical replicates per condition). The black line is a linear fit extrapolated from the mean fluorescence at 0.05 to 0.2mM. Blue circles represent the normalized stress response capacity (see Methods for detail). **g.** Resistance, tolerance and peak stress-response as a function of $[H_2O_2]$, normalized from Fig1c, 1d and 1f respectively (also see Methods). Lines are logistic fits for resistance and stress response and a second order power law for tolerance. **h.** Boxplot of the Srx1pr-GFP-deg peak response (at t=1h following stress addition) in resistant versus non-resistant cells. **i.** Same as **h**, but for tolerant versus non-tolerant cells. The blue dashed line represents the responder threshold (see Methods for detailed). Statistical differences (two-sided Wilcoxon rank sum test) are indicated by *** for $p < 0.001$, NS for $p > 0.05$. Insets in panel **h** and **i**: sketches explaining the principle of the combined measurement of responder cells and resistant (resp. tolerant) cells in the resistance (resp. tolerance) assays.

Fig. 2: Investigating the genetic determinism of resistance and tolerance unravels a trade-off between the two defense strategies

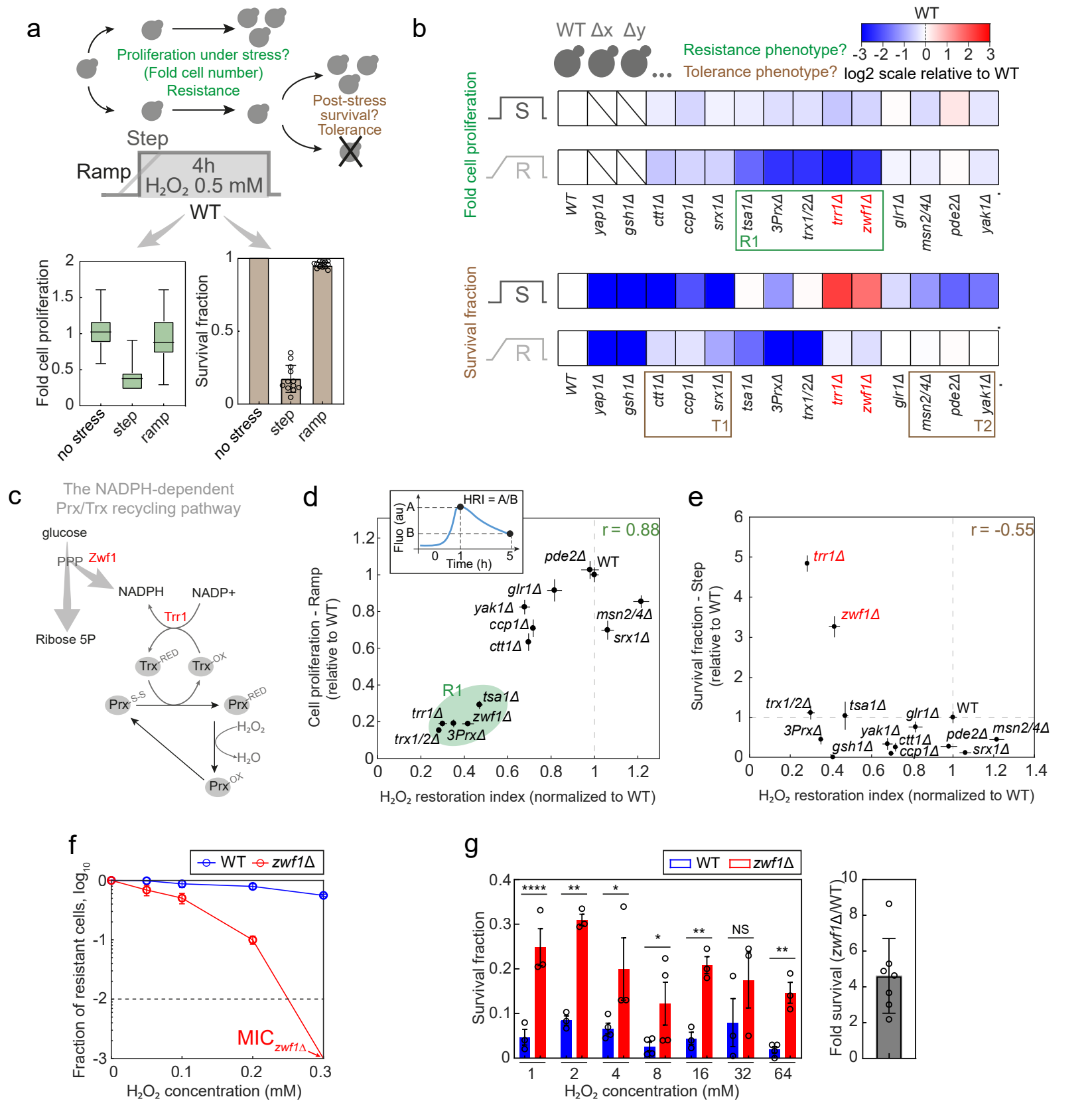

Figure 2: Investigating the genetic determinism of resistance and tolerance unravels a trade-off between the two defense strategies

a, Top panel : sketch of the step and ramp stress assays used to measure resistance and tolerance. Bottom left panel: normalized cell proliferation under stress (based on n=55 micro-colonies, see Methods for details) for steps and ramps in WT cells; Bottom right panel: post-stress survival for steps and ramps in WT cells (N = 12 independent replicates, n>100 for each replicate). **b,** Top panel: Quantification of the normalized cell proliferation both in the step and the ramp assays for the indicated mutants (between n = 6 and 55 micro-colonies depending on mutants). Bottom panel: quantification of the post-stress survival both in the step and the ramp assays for the indicated mutants (N = 3 technical replicates for each condition). The green rectangle R1 represents a group of mutants with low resistance. The brown rectangles T1 and T2 represent two groups of mutants with low tolerance. **c,** Sketch of the NADPH-dependent Prx/Trx recycling pathway. **d,** Normalized cell proliferation during ramps (as in **b**) as a function of the H_2O_2 restoration index (HRI), normalized to WT. r indicates the correlation coefficient. Error bars represent the s.e.m (N=3 replicates). n>50 single-cells for HRI measurements. **e,** Quantification of the post-stress survival in response to the step assay (from (b)) as a function of the H_2O_2 restoration index, normalized to WT. r indicates the correlation coefficient. Error bars represent the s.e.m, N=3 replicates for tolerance and n>50 single-cells for HRI measurements. **f,** Fraction of resistant cells in WT (blue) and *zwf1*Δ (red) cells as a function of H_2O_2 concentration. **g,** Left panel: Survival fraction of WT (blue) and *zwf1*Δ (red) cells as a function of H_2O_2 concentration. For each concentration, the duration of stress exposure is set to the WT MDK99 (see Extended data Fig. 1a). N = 3 to 4 technical replicates, n>100 for each replicate. Statistical differences (one-sided two-sample t-test) are indicated by **** for $p < 0.0001$, *** for $p < 0.001$, ** for $p < 0.01$, * for $p < 0.05$, NS for $p > 0.05$. Right panel: Fold change in *zwf1*Δ survival versus WT after pooling all tested concentrations in the left panel.

Fig. 3: Proliferation and survival are antagonistic features of the oxidative stress response

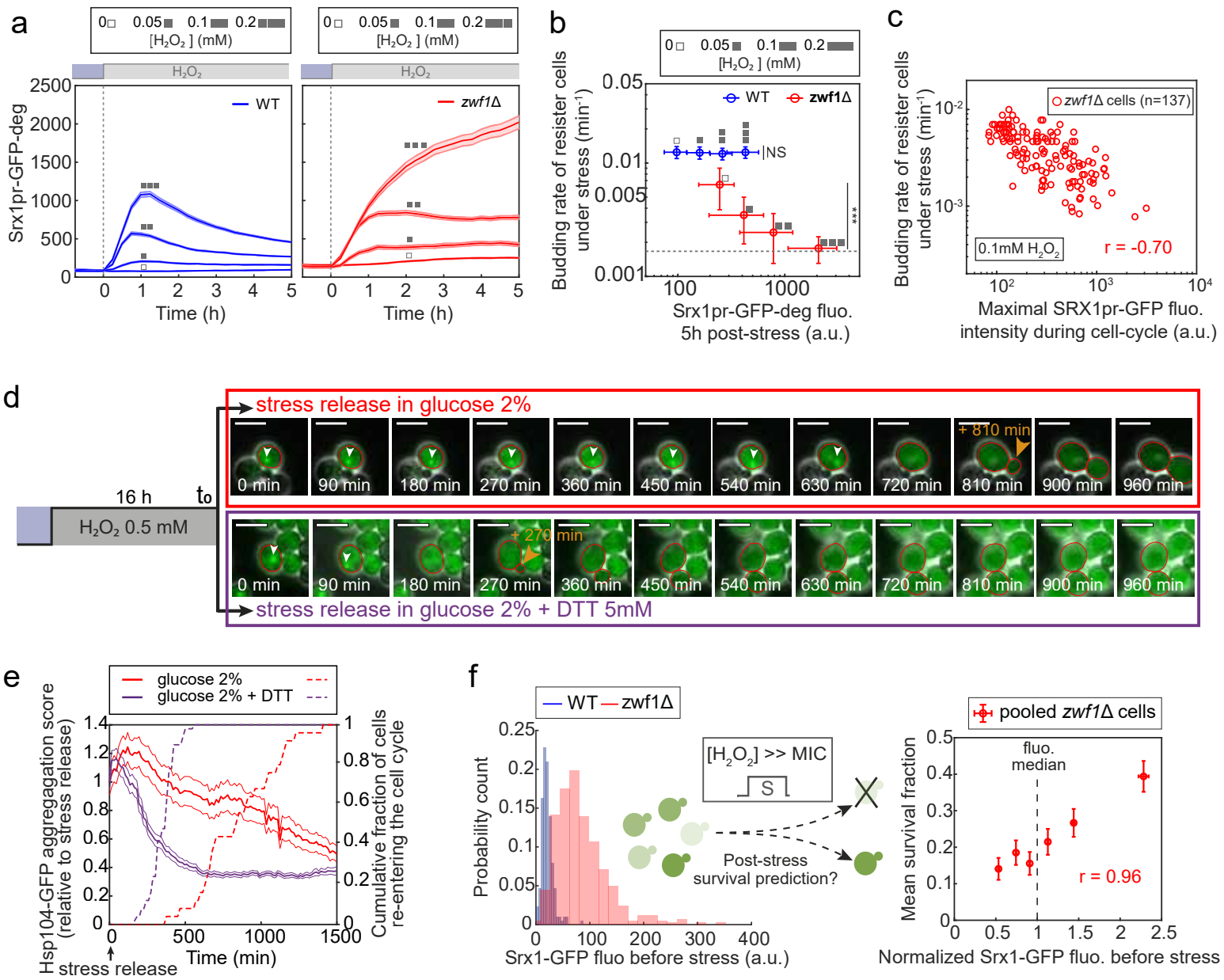

Figure 3: Proliferation and survival are antagonistic features of the oxidative stress response

a. Quantification of the mean Srx1pr-GFP-deg fluorescence expression +/- s.e.m. over time in WT (blue) and *zwf1*Δ mutant (red) in response to the indicated H_2O_2 concentrations. **b.** Mean budding rate of resistant cells +/- one standard deviation (n>33 single-cells per condition) as a function of the mean Srx1pr-GFP-deg fluorescence expression after 5h under stress +/- one standard deviation in WT (blue, n>100) and zwf1Δ mutant (red, n>100). Statistical differences in budding-rates from 0 to 0.2 mM were evaluated for WT and *zwf1*Δ strains using a one-way ANOVA test for multiple comparisons. **** for $p < 0.0001$, *** for $p < 0.001$, ** for $p < 0.01$, * for $p < 0.05$, NS for $p > 0.05$. **c.** Budding rate of individual *zwf1*Δ cells exposed to 0.1 mM for more than 5h as a function of the maximal fluorescence expression of the SRX1pr-GFP-deg reporter during the corresponding cell cycle (n=137). *r* is the correlation coefficient between both quantities. **d.** Time series showing phase contrast and GFP fluorescence images of *zwf1*Δ cells (red contours) carrying an Hsp104-GFP reporter cell after release into the indicated media (following an initial 16 h long exposure to 0.5 mM H_2O_2). White arrows indicate the Hsp104-GFP aggregates. The orange arrow at the indicated time marks the first bud observed after stress release. Scale bar 6.2 µm. **e.** Hsp104-GFP aggregation score +/- s.e.m., normalized to the aggregation score at t=0min, following stress release as in **d**. Only surviving cells are included in the analysis (see Methods, n>50 for each condition at all times). Cumulative fraction of cells re-entering the cell-cycle with (red, n=35) or without (purple, n=50) DTT addition (see Methods for detail). **f.** Left panel: distribution of basal fluorescence of the Srx1-GFP fusion protein in WT and *zwf1*Δ strains (n=807 cells) at the onset of a 7.5 or 15 min stress exposure at 64 mM H_2O_2. Right panel: Mean survival in *zwf1*Δ cells from **f** sorted by their normalized pre-stress Srx1-GFP signal +/- s.e.m (n=135 cells for group 1 to 5 and n= 132 cells for group 6). Data were pooled into 6 bins according to the initial Srx1-GFP level of the cells. *r* is the correlation coefficient between both parameters.

Fig. 4: Stress tolerance requires the Prx/Trx pathway to drive PKA inhibition

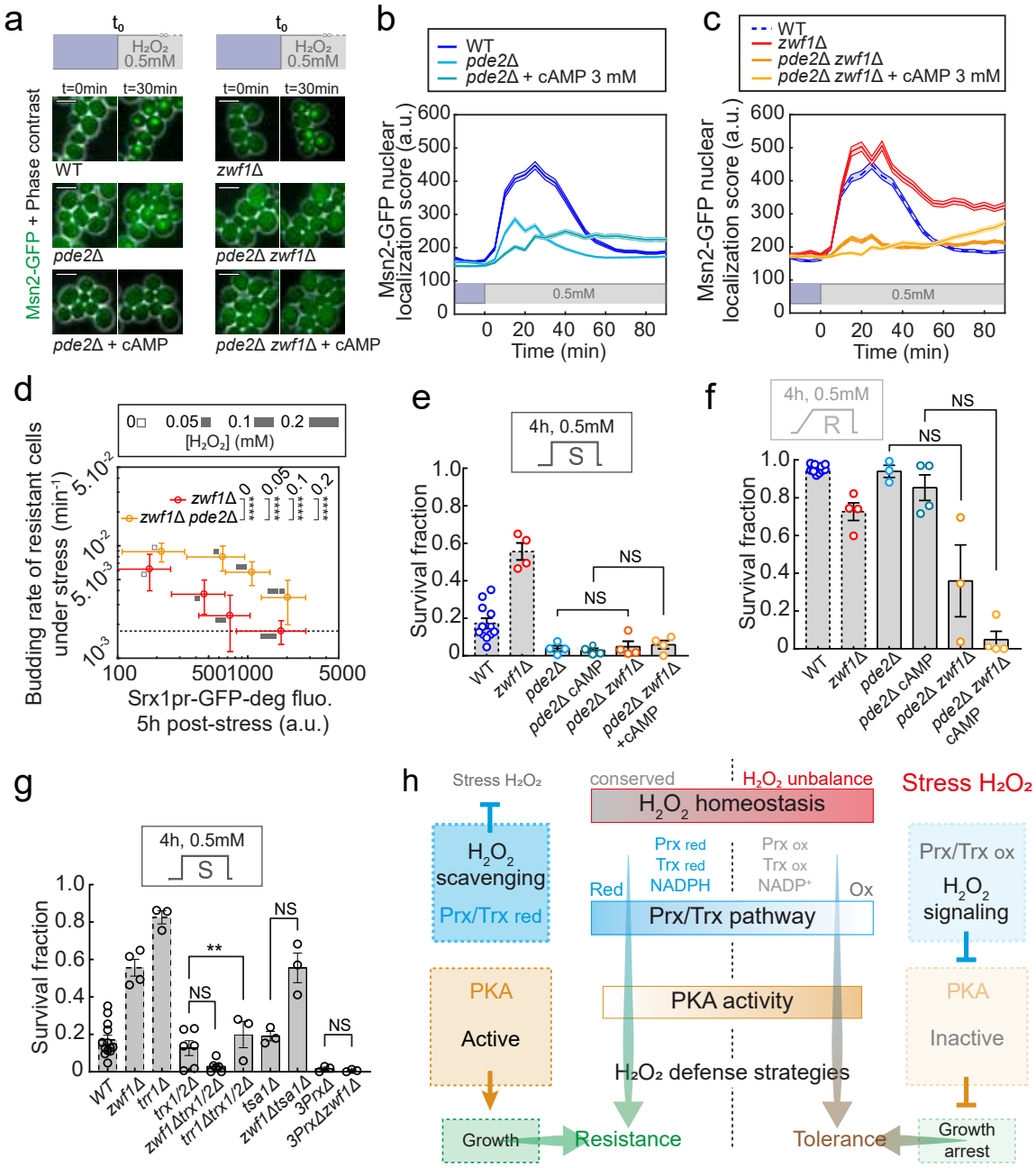

Fig. 4: Stress tolerance requires thioredoxins to drive PKA inhibition

a, Overlays of phase-contrast and fluorescence images of cells carrying a Msn2-GFP fusion before (t=0min) and after (t=30min) the addition of 0.5 mM H_2O_2 for the indicated strains. Scale bar: 6.2µm. Stripes represent the stress pattern. **b,c,** Nuclear localization score of Msn2-GFP over time +/- s.e.m. for the identical strain background. The WT dash-line in **(c)** is identical as that in **(b)**. **d,** Mean budding rate under stress +/- std as a function of the mean SRX1pr-GFP-deg expression +/- std under different H_2O_2 stress conditions (from 0 to 0.2 mM) for the indicated strains. All the cells with a budding rate smaller than 0.0017 min^{-1} (dashed line) were discarded in this analysis. Statistical differences were evaluated between zwf1Δ and zwf1Δpde2Δ strains at each H_2O_2 concentration using a two-sided Man Whitney U test. **** for $p < 0.0001$, NS for $p > 0.05$. **e-g,** Survival fraction in response to a 4 h 0.5 mM H_2O_2 step (**e** and **g**) or ramp (**f**) exposure for the indicated strain backgrounds. Bars represent means of independent technical replicates (open circles, n>100 for each replicate). Error bars indicate the s.e.m.. Dashes bars represent data displayed in Fig. 2. The statistical analysis is based on a one-sided t-test with **** for $p < 0.0001$, *** for $p < 0.001$, ** for $p < 0.01$, * for $p < 0.05$, NS for $p > 0.05$. **h,** Sketch of the model illustrating the switch between resistance and tolerance. When H_2O_2 homeostasis can be achieved, Prx/Trx are mostly reduced, PKA is active and cell maintain their proliferation (resistance regime). When the internal H_2O_2 level overcomes the cell's scavenging capabilities, Prx/Trx are mostly oxidized, thus inactiving PKA and enabling cell survival by arresting cell growth (tolerance regime). .

Fig. 5: Stress tolerance restricts cell death in glucose-depleted cells, despite their inability to maintain H_2O_2 homeostasis

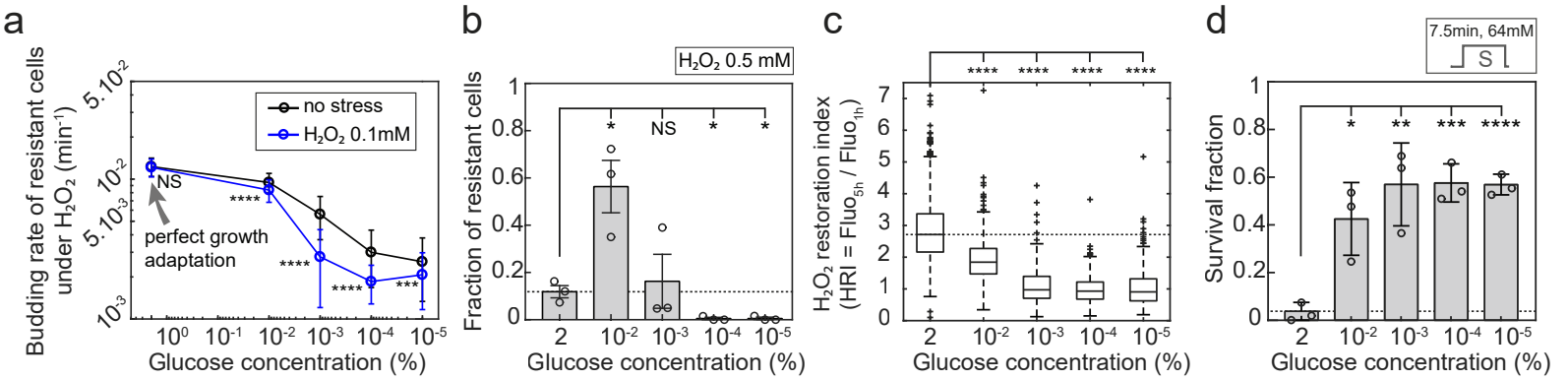

Fig. 5: Glucose limitation increases thre survival of the cells, despite their inability to maintain H_2O_2 homeostasis.

a, Mean budding rate of resistant cells +/- std without (black line, n>62 cells per data point) or with 0.1 mM H_2O_2 (blue line, n>61 per condition) for more than 5 h as a function of glucose concentration. The statistical analysis is based on a two-sided Man Whitney U test. **b,** Fraction of resistant cells during a 0.5 mM H_2O_2 stress. Open circles are independent technical replicates (N = 3 with n>100 for each replicate); bars represent the mean value and the error bars are the s.e.m. The statistical analysis is based on a two-sided t-test. **c,** H_2O_2 restoration index (HRI) under 0.1 mM H_2O_2 as a function of glucose concentration. The statistical analysis is based on a two-sided Man Whitney U test. **d** Fraction of tolerant cells after a 64 mM H_2O_2 stress exposure for 7.5 min. Open circles are independent technical replicates (N = 3 with n>100 for each replicate), bars represent the mean value and the error bars are the s.e.m. The statistical analysis is based on a two-sided t-test. For all the panels, significance levels are: **** for $p < 0.0001$, *** for $p < 0.001$, ** for $p < 0.01$, * for $p < 0.05$, NS for $p > 0.05$.

Fig. 6: The trade-off between H2O2 resistance and tolerance in G6PDH-deficient cells is conserved in the prokaryote E. coli

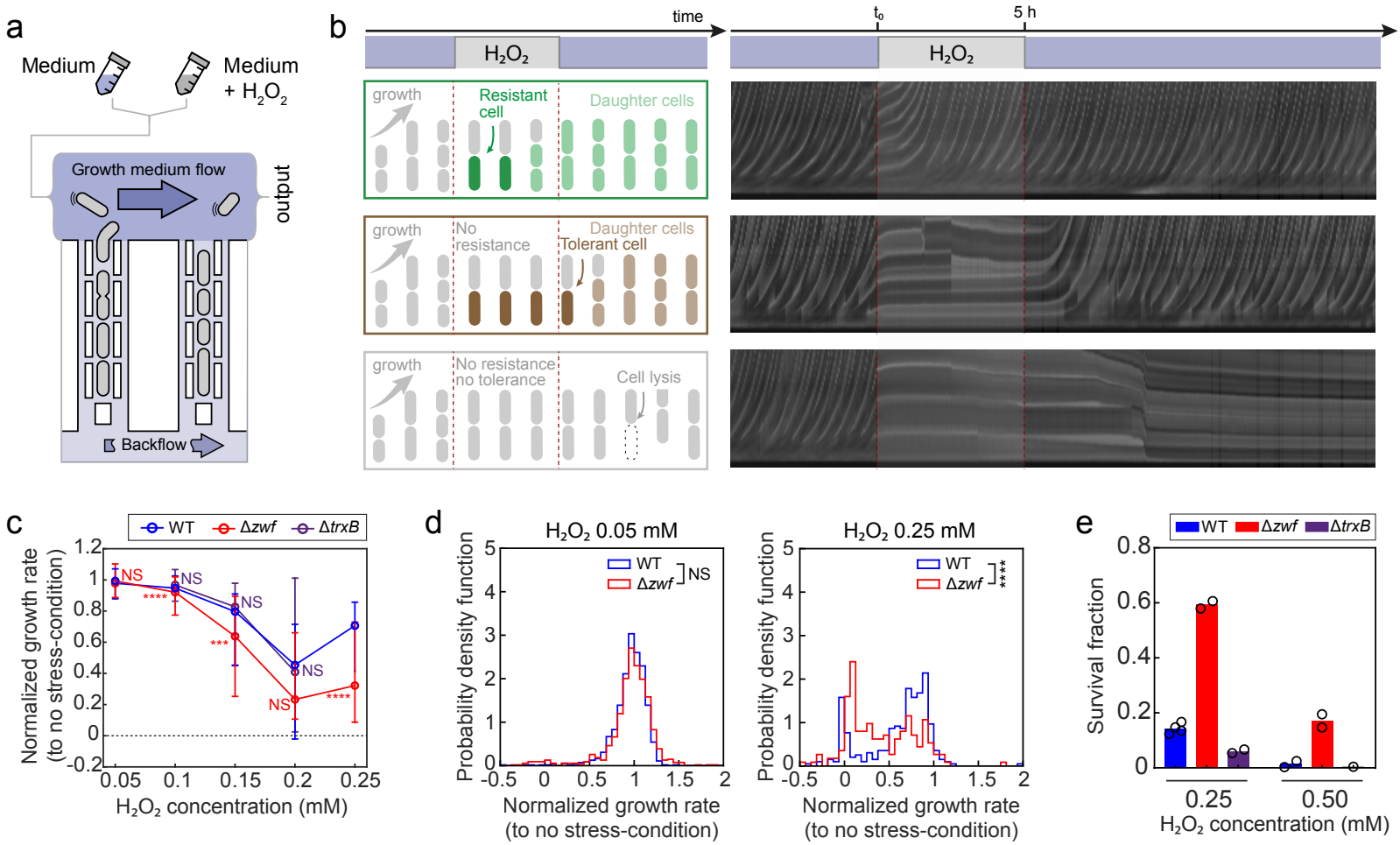

Fig. 6: The trade-off between H_2O_2 resistance and tolerance in G6PDH-deficient cells is conserved in the prokaryote *E. coli*

a, Sketch of the improved mother-machine microfluidic device used to image *E. coli* cells during and after an H_2O_2 stress exposure. **b,** Representative kymographs of three individual cell traps during an exposure to a 0.25mM H_2O_2 stress over 5h. Each kymorgaph represents a particular cell fate (resistance, tolerance, or death). **c,** Normalized median normalized growth rate of cells (relative to the no stress control) as a function of H_2O_2 concentration (n>105 for WT, n>185 for Δ*zwf*, and n>90 for ΔtrxB). Error bars represent quartiles. **d,** Probability density function of the normalized growth rate shown in **(c)** at 0.05 and 0.25 mM H_2O_2, in WT and Δ*zwf* strains. **c,d,** Statistical analysis employed one-sided Man Whitney U tests, **** for $p < 0.0001$, *** for $p < 0.001$, ** for $p < 0.01$, * for $p < 0.05$, NS for $p > 0.05$. **e,** Survival fraction in response to boluses of H_2O_2 (0.25 or 0.5 mM for 5 h). Open circles are technical replicates (N = 2 to 4 replicates for WT and Δ*zwf* and Δ*trxB* at 0.25 mM. Only one replicate for ΔtrxB at 0.5 mM since all cells were almost dead at 0.25 mM).

Extended Data Fig. 1

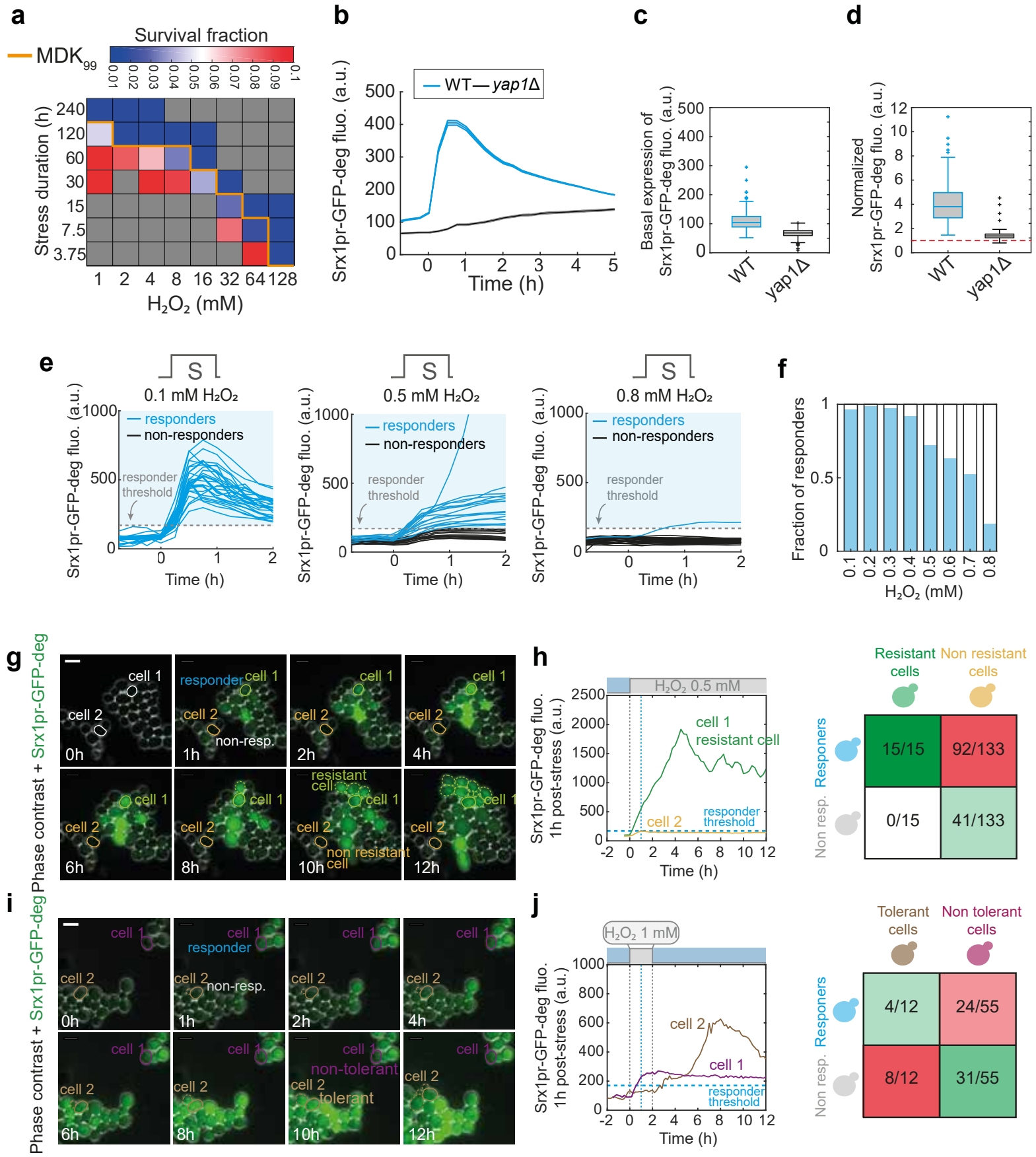

Extended data Fig. 1: a, Heatmap of the fraction of survival cells as a function of H_2O_2 concentration and time under stress (N≥2 for each tested condition). Grey squares are non-tested conditions. The yellow line delineates the MDK99 (minimal duration to kill 99% of the cells). **b,** Mean Srx1pr-GFP-deg fluorescence +/- s.e.m. in WT and *yap1*Δ strains in response to 0.1mM H_2O_2 (n>100 single-cells for each strain). **c,** Boxplot of the basal expression (before stress exposure) of Srx1-GFP-deg in WT (n=337) and *yap1*Δ (n=118). **d,** Upregulation of Srx1pr-GFP-degron upon a 1h stress exposure. Boxplots indicate the normalized fluorescence at t=1h over the basal fluorescence (t=0h) for WT (n=334) and *yap1*Δ (n=114) cells. **e,** Single-cell trajectories of Srx1-GFP-deg cells at indicated H_2O_2 concentrations for responding cells (blue lines) and non-responding cells (black lines). The gray dashed line indicates the "responder" threshold (see Methods for detail). **f,** Fraction of responding cells as a function of H_2O_2 concentration (n>500 single-cells, pooled from at least N=2 technical replicates) **g,** Sequence of overlaid phase contrast and fluorescence images of WT cells carrying an Srx1pr-GFP-deg reporter. Green (resp. orange) contours indicate typical resistant (resp. non-resistant) cells. **h,** Left: quantification of cytoplasmic fluorescence of cells indicated in panel **g**; Right: confusion matrix showing the fraction of responding and non-responding cells for both resistant and non resistant cells. **i,j,** Same as **g** and **h**, but upon a tolerance assay (2 hours H_2O_2 at 0.1mM).

Extended Data Fig. 2

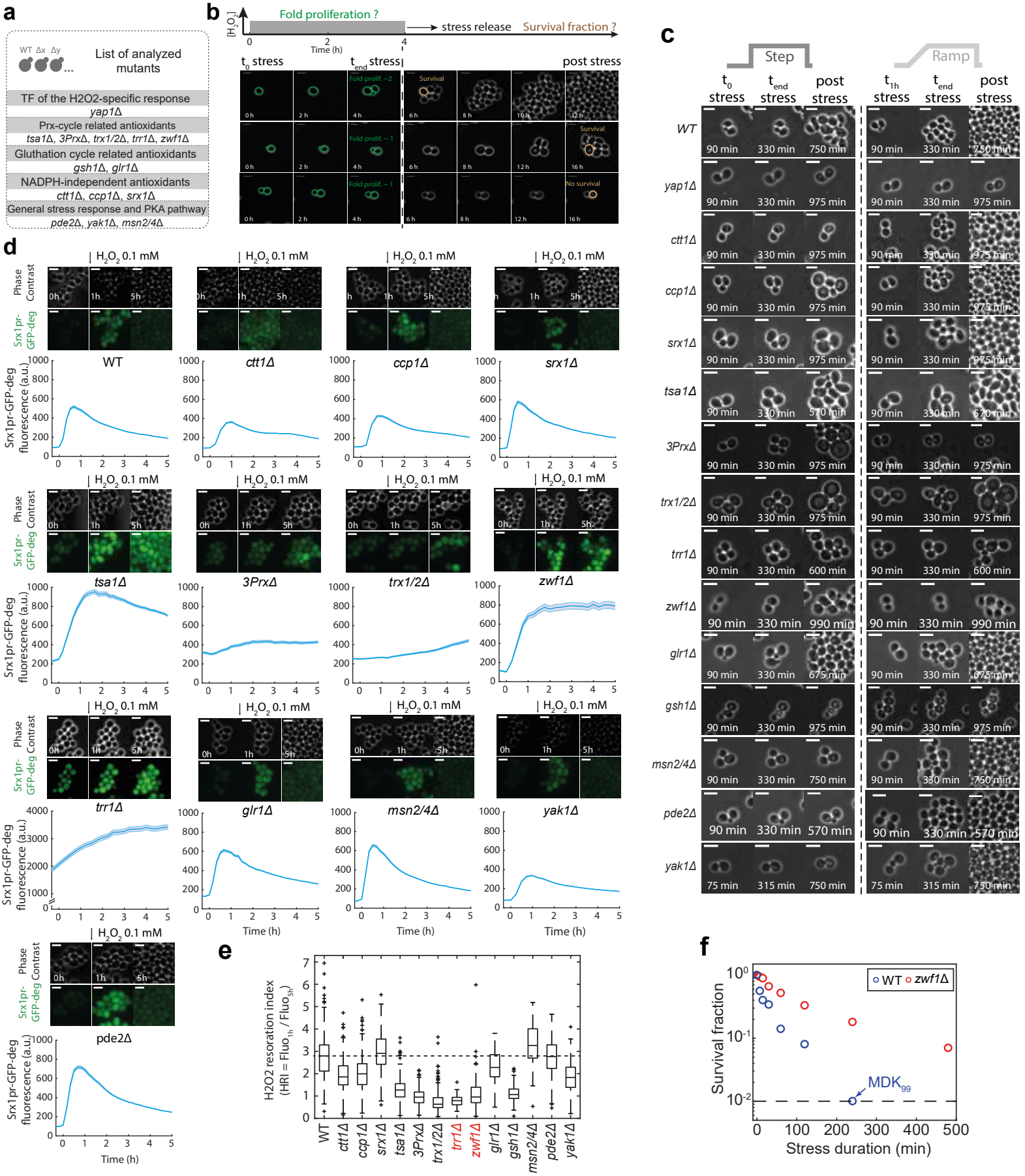

Extended data Fig. 2:

a, List of the mutant strains analyzed in this study. **b,** Sequences of phase contrast images of representative WT resistant (top), tolerant (middle), and dead (bottom) cells; **c,** Sequence of images showing representative cells of the indicated background. Scale bar: 6.2 µm. **d,** Sequence of phase contrast and Srx1pr-GFP-degron fluorescence images (top) and quantification of the mean Srx1pr-GFP-deg expression +/- s.e.m. of a population of cells with the indicated background during a continuous 0.1 mM H_2O_2 exposure; **e,** Boxplot of the H_2O_2 restoration index (HRI = Fluo(1h) / Fluo(5h)) for the indicated mutant strains. **f,** Survival fraction of the WT (blue) and *zwf1Δ* mutant (red) as a function of stress duration at 1 mM. MDK99 is defined as the smallest duration whereby less than 1% cells survive.

Extended Data Fig. 3

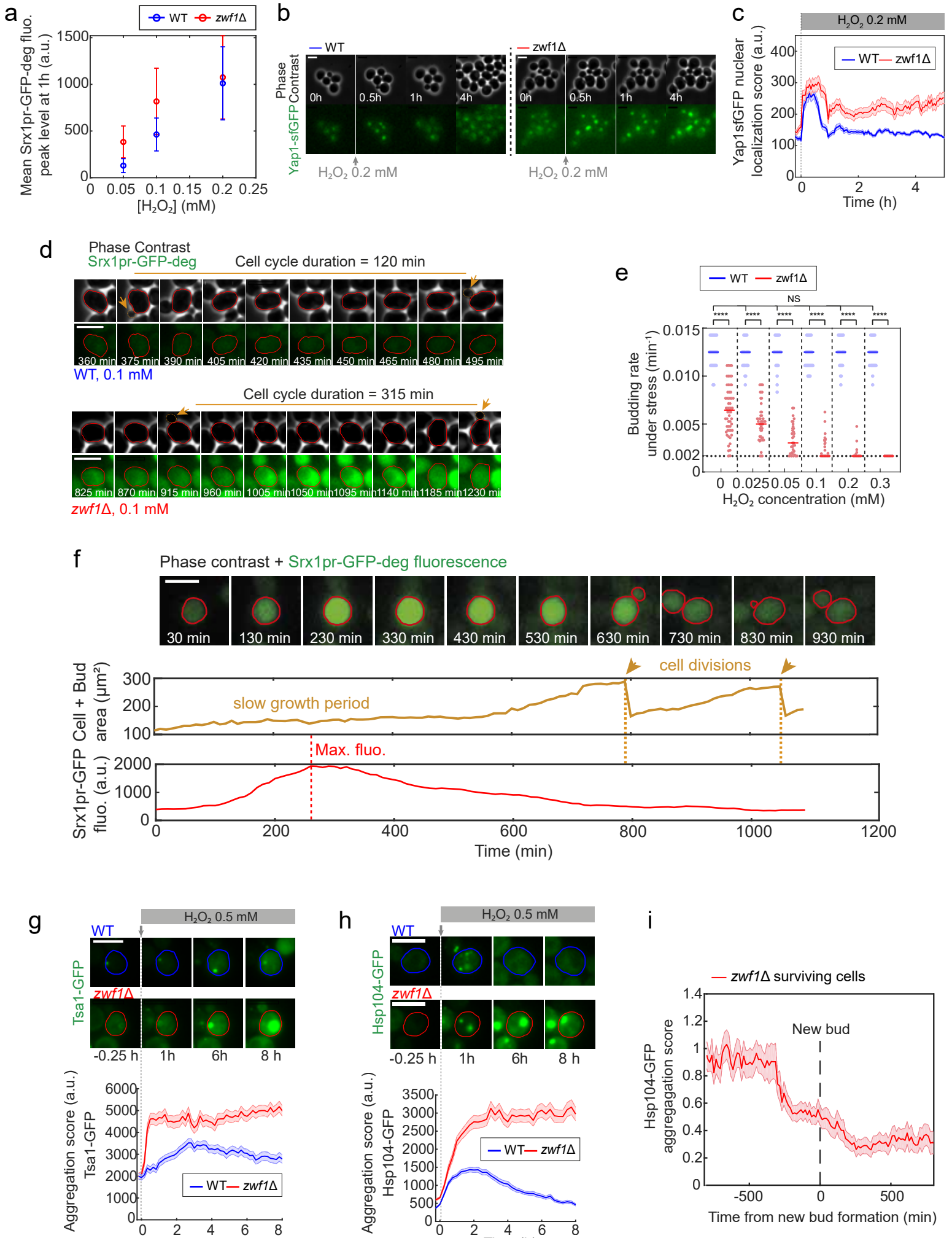

Extended data Fig. 3:

a, Mean Srx1pr-GFP-deg fluorescence +/- std measured 1 h after the onset of stress exposure in WT and *zwf1Δ* strains as a function of H_2O_2 concentration. **b,** Sequence of phase contrast and Yap1-sfGFP fluorescence in WT and *zwf1Δ* strains in response to a 0.2 mM H_2O_2 exposure. **c,** Yap1-sfGFP nuclear localization score +/- s.e.m. in WT and *zwf1Δ* cells measured from the experiment in **b**. The vertical dashed line indicates the onset of stress exposure. **d,** Sequence of phase contrast and Srx1pr-GFP-deg fluorescence of WT and zwf1Δ cells continuously exposed to a 0.1 mM H_2O_2 stress. Orange arrows indicate budding events. **e,** Budding rates of WT (blue symbols) and *zwf1Δ* (red symbols) cells as a function of H_2O_2 concentration; each filled symbol corresponds to a single cell; horizontal colored lines represent the median budding rate. All the cell cycles with a frequency smaller than 0.0017 min^{-1} were included in the analysis as of a frequency of 0.0017 min^{-1} Statistical differences (two-sided Mann-Whitney U test) are indicated by **** for $p < 0.0001$, NS for $p > 0.05$. **f,** Top panel: sequence of overlaid phase contrast and Srx1pr-GFP-deg fluorescence of a representative *zwf1Δ* cell during one cell cycle in the absence of H_2O_2 stress. Bottom panel: quantification of cell and bud area (top) as well as Srx1pr-GFP-degron fluorescence (bottom) over time. The red vertical dashed line shows the time when the cell reaches a fluorescence maximum. **g,** Top: sequence of Tsa1-GFP fluorescence images for WT and *zwf1Δ* cells at indicated times; Bottom: quantification of the aggregation score +/- s.e.m. of Tsa1-GFP foci for the indicated strains. **h,** Same as g, but for the Hsp104-GFP reporter**.** The dashed line indicates the onset of stress exposure. **i,** Mean Hsp104-GFP aggregation score +/- s.e.m. after stress release in the population of surviving *zwf1Δ* cells, after synchronization from new bud formation for each single cell.

Extended Data Fig. 4

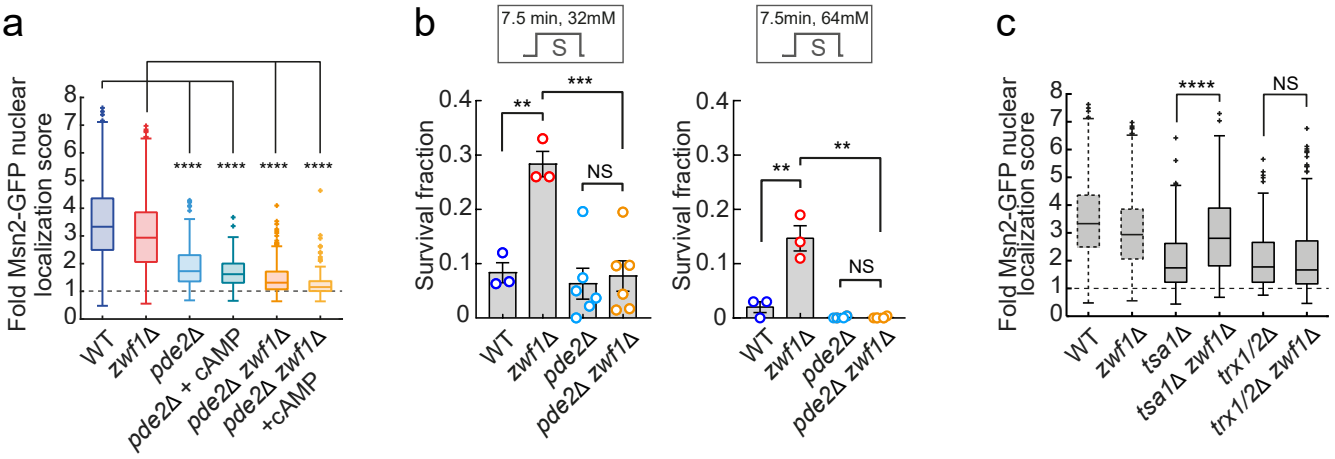

Extended data Fig. 4:

a, Boxplots of the fold increase in the Msn2-GFP nuclear score between the no-stress condition and 30 min after stress the addition of a XXmM H_2O_2 dose (n>100 for each condition). Statistical analysis based on a two-sided Mann-Whitney U test. **b,** Survival fraction in response to H_2O_2 boluses (32 or 64 mM for 7.5 min). Filled circles represent independent technical replicates (N = 3 to 6, n>100 for each replicate), error bars are s.e.m. Statistical analysis is based on a one-sided t-test for comparison between WT and *zwf1*Δ and between *pde2*Δ and *zwf1*Δ*pde2*Δ, and a two-sided t-test for comparison between *zwf1*Δ and *zwf1*Δ*pde2*Δ (no assumption was made on the effect of *PDE2* deletion in the *zwf1*Δ background). **c**, same as **a**, for different strain background; The dashed boxplots are identical to the WT and *zwf1*Δ ones on a; **a-c,** **** for $p < 0.0001$, *** for $p < 0.001$, ** for $p < 0.01$, * for $p < 0.05$, NS for $p > 0.05$.

Extended Data Fig. 5

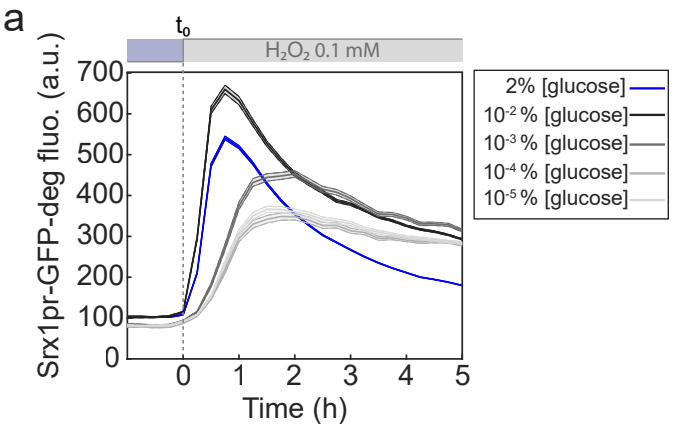

Extended data Fig. 5:

a, Mean Srx1pr-GFP-deg fluorescence +/- s.e.m. over time in response to a 0.1 mM H_2O_2 stress for different glucose concentrations.

Extended Data Fig. 6

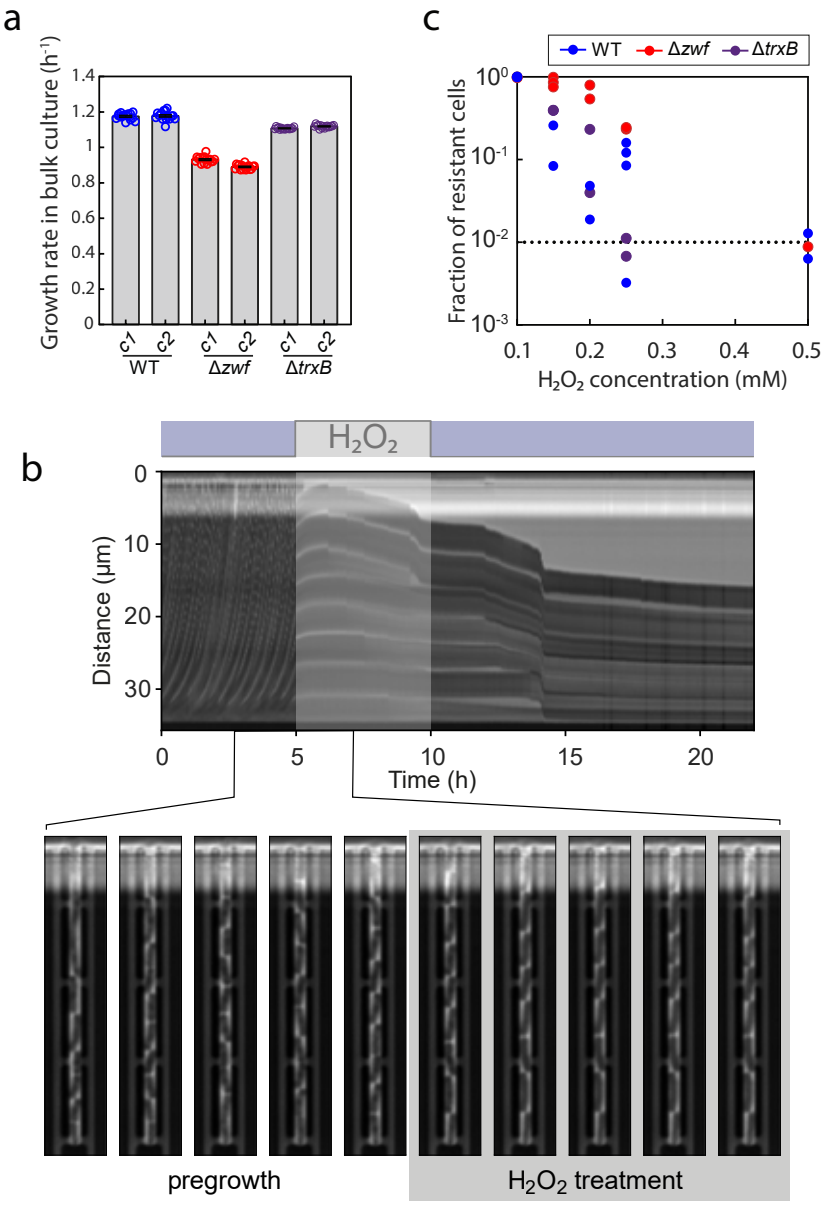

Extended data Fig. 6:

a, Growth rate of WT, Δ*zwf* and Δ*trxB* strains in liquid cultures. c1 and c2 are two different clones. Circles show the different technical replicates and the gray bars indicate the mean over the replicates. **b,** Sequence of raw phase contrast images of *E. coli* cells in the microfluidic device (bottom) and reduction of the dimensionality using a kymograph (top image). **c,** Fraction of resistant cells in WT, Δ*zwf* and Δ*trxB* strains. Circles represent technical replicates (N = 2 to 4 for concentrations close to the MIC). The dashed line indicates a 1% survival, from which the MIC can be calculated.